Numerische
Mathematik

A second-order positivity preserving central-upwind scheme for chemotaxis and haptotaxis models

Alina Chertock · Alexander Kurganov

Abstract The paper is concerned with development of a new finite-volume method for a class of chemotaxis models and for a closely related haptotaxis model. In its simplest form, the chemotaxis model is described by a system of nonlinear PDEs: a convection-diffusion equation for the cell density coupled with a reaction-diffusion equation for the chemoattractant concentration. The first step in the derivation of the new method is made by adding an equation for the chemoattractant concentration gradient to the original system. We then show that the convective part of the resulting system is typically of a mixed hyperbolic-elliptic type and therefore straightforward numerical methods for the studied system may be unstable. The proposed method is based on the application of the second-order central-upwind scheme, originally developed for hyperbolic systems of conservation laws in Kurganov et al. (SIAM J Sci Comput 21:707–740, 2001), to the extended system of PDEs. We show that the proposed second-order scheme is positivity preserving, which is a very important stability property of the method. The scheme is applied to a number of two-dimensional problems including the most commonly used Keller–Segel chemotaxis model and its modern extensions as well as to a haptotaxis system modeling tumor invasion into surrounding healthy tissue. Our numerical results demonstrate high accuracy, stability, and robustness of the proposed scheme.

Mathematics Subject Classification (2000) 76M12 · 92C17 · 35M10

A. Chertock (✉)
Department of Mathematics, North Carolina State University, Raleigh, NC 27695, USA
e-mail: chertock@math.ncsu.edu

A. Kurganov
Mathematics Department, Tulane University, New Orleans, LA 70118, USA
e-mail: kurganov@math.tulane.edu

1 Introduction

This paper is focused on designing a new numerical method for a class of two-dimensional (2D) systems of advection-reaction-diffusion equations describing chemotaxis models [13,25–27,41,44,50,51] and a closely related haptotaxis model [2,10,11].

We begin with the most common formulation of the Keller–Segel system [13], which can be written in the dimensionless form as:

$$u_t + \nabla \cdot (\chi u \nabla v) = \Delta u, \tag{1.1}$$

$$v_t = \Delta v - v + u. \tag{1.2}$$

Here, $u(x, y, t)$ denotes the cell density, $v(x, y, t)$ stands for a chemoattractant concentration, and χ is a chemotactic sensitivity constant. It is well-known that solutions of the system (1.1) and (1.2) may blow up in finite time, see, e.g., [9,22,23,45] and the references therein. This blow-up represents a mathematical description of a cell concentration phenomenon that occur in real biological systems, see, e.g., [1,6–8,14,46,54].

The Keller–Segel model (1.1) and (1.2) can be generalized to better describe the reality by taking into account several additional factors. For instance, one may consider a more complicated (than just a constant) and a more realistic chemotactic sensitivity function, $\chi = \chi(u, v)$, in (1.1) as, e.g, in [21,25,38,50,51]. Some other factors, such as growth and death of cells, more accurate [than on the right-hand side (RHS) of (1.2)] terms describing production and uptake of the chemoattractant by cells, presence of food and other chemicals in the system, may also be incorporated into the chemotaxis model, see, e.g., [50,51].

A common property of all existing chemotaxis systems is their ability to model a concentration phenomenon that mathematically results in solutions rapidly growing in small neighborhoods of concentration points/curves. The solutions may blow up or may exhibit a very singular, spiky behavior. In either case, capturing such singular solutions numerically is a challenging problem. Several numerical methods for a simpler version of the Keller–Segel model,

$$\begin{cases} u_t + \nabla \cdot (\chi u \nabla v) = \Delta u, \\ \Delta v - v + u = 0, \end{cases}$$

have been proposed in [15,40,48]. In this model, Eq. (1.2) has been replaced by an elliptic equation using an assumption that the chemoattractant concentration v changes over much smaller time scales than the cell density u. A fractional step numerical method for a fully time-dependent chemotaxis system from [51] has been proposed in [52] (see also [39] for an application of the fractional step method to related models of angiogenesis and vasculogenesis). However, the fractional step (operator splitting) approach may not be applicable in the case when the convective part of the chemotaxis system is not hyperbolic, which is a generic situation as we demonstrate below. Thus, there is a need in accurate and robust numerical methods for general chemotaxis models, especially since many interesting theoretical questions are still completely open due to the lack of reliable numerical tools.

In this paper, we provide a simple mathematical explanation on why a naïve numerical approach for, say, the system (1.1) and (1.2) may not be able to capture its blowing up solutions. To this end, we differentiate equation (1.2) with respect to x and y and then rewrite the system (1.1) and (1.2) as:

$$\begin{cases} u_t + \nabla \cdot (\chi u \mathbf{w}) = \Delta u, \\ \mathbf{w}_t - \nabla u = \Delta \mathbf{w} - \mathbf{w}, \end{cases} \tag{1.3}$$

where $\mathbf{w} := \nabla v$. In Sect. 2, we show that the convective part of the system (1.3),

$$\begin{cases} u_t + \nabla \cdot (\chi u \mathbf{w}) = 0, \\ \mathbf{w}_t - \nabla u = 0, \end{cases} \tag{1.4}$$

is generically of a mixed, hyperbolic-elliptic type. Moreover, in the hyperbolic region, the propagation speeds are generically larger than $|v_x|$ and $|v_y|$. A numerical method that does not employ this information may obviously be unstable, as it is demonstrated in Sects. 3.1 and 3.2.

The main goal of this paper is to develop an accurate and robust numerical method for the Keller–Segel system and related models. We design a scheme, which is both second-order accurate and positivity preserving. The former property ensures a high resolution of the numerical solution, while the latter property (positivity of the computed cell densities u) is very important since appearance of negative values of u may trigger numerical instabilities as demonstrated in Sects. 3.1 and 3.2. We would like to emphasize that designing a numerical method, which preserves positivity for a second-order scheme is, in general, a nontrivial task and, for the best of our knowledge, the central-upwind scheme, we propose here, is the first one to achieve this goal.

The new method is constructed by applying a second-order Godunov-type central-upwind scheme from [32] to the system (1.3). Central-upwind schemes have been originally developed in [31,32,34] for hyperbolic systems of conservation laws. They have also been successfully applied to convection-diffusion equations [12,34] and systems of balance laws [29,30,33]. Central-upwind schemes are Godunov-type finite-volume methods that, unlike the original first-order Godunov scheme [17] and its higher-order upwind extensions (see, e.g., [16,28,35,36]), do not employ a characteristic decomposition and/or (approximate) solutions of (generalized) Riemann problems and thus can be applied as a "black-box-solver" to a wide variety of (systems of) time-dependent PDEs.

Since (1.4) is not necessarily hyperbolic, the central-upwind scheme has to be modified while applied to the system (1.3) and therefore, we design an extension of the second-order central-upwind scheme for this system. We prove that the resulting second-order method globally preserves positivity of the computed values of the density u (see Sect. 2.1).

In Sect. 3.1, we test the proposed method on the classical Keller–Segel model. In Sects. 3.2 and 3.3, the new method is applied to a more realistic chemotaxis model from [50,51] and in Sect. 3.4, it is implemented to the haptotaxis model from [2,10,11]. Our numerical experiments clearly demonstrate high resolution, stability and robustness of the designed central-upwind scheme.

2 Derivation of the scheme

In this section, we derive a central-upwind scheme for the Keller–Segel system (1.1) and (1.2). As it was mentioned above, we first differentiate equation (1.2) with respect to x and y and rewrite the system as (1.3), which in the coordinate form reads:

$$\begin{cases} u_t + (\chi u p)_x + (\chi u q)_y = u_{xx} + u_{yy}, \\ p_t - u_x = p_{xx} + p_{yy} - p, \\ q_t - u_y = q_{xx} + q_{yy} - q, \end{cases} \tag{2.1}$$

where $(p, q)^T := \mathbf{w} = \nabla v$. This system can be viewed as a system of advection-reaction-diffusion equations:

$$\mathbf{U}_t + \mathbf{f}(\mathbf{U})_x + \mathbf{g}(\mathbf{U})_y = \Delta \mathbf{U} + \mathbf{R}(\mathbf{U}), \tag{2.2}$$

where $\mathbf{U} := (u, p, q)^T$, $\mathbf{f}(\mathbf{U}) := (\chi u p, -u, 0)^T$, $\mathbf{g}(\mathbf{U}) := (\chi u q, 0, -u)^T$, and $\mathbf{R}(\mathbf{U}) := (0, -p, -q)^T$. The Jacobians of $\mathbf{f}$ and $\mathbf{g}$ are:

$$\frac{\partial \mathbf{f}}{\partial \mathbf{U}} = \begin{pmatrix} \chi p & \chi u & 0 \\ -1 & 0 & 0 \\ 0 & 0 & 0 \end{pmatrix} \quad \text{and} \quad \frac{\partial \mathbf{g}}{\partial \mathbf{U}} = \begin{pmatrix} \chi q & 0 & \chi u \\ 0 & 0 & 0 \\ -1 & 0 & 0 \end{pmatrix},$$

and their eigenvalues are:

$$\lambda^{\mathbf{f}}_{1,2} = \frac{\chi}{2}\left(p \pm \sqrt{p^2 - \frac{4u}{\chi}}\right), \lambda^{\mathbf{f}}_3 = 0 \quad \text{and} \quad \lambda^{\mathbf{g}}_{1,2} = \frac{\chi}{2}\left(q \pm \sqrt{q^2 - \frac{4u}{\chi}}\right), \lambda^{\mathbf{g}}_3 = 0, \tag{2.3}$$

respectively. It is now clear that the "purely" convective system (1.4) is hyperbolic only if both $\chi p^2 \geq 4u$ and $\chi q^2 \geq 4u$ (otherwise, it is elliptic). Unfortunately, the ellipticity condition, $\chi \min(p^2, q^2) < 4u$, is satisfied in generic cases, for example, when $p = v_x = 0$ and $u > 0$. Therefore, the operator splitting (fractional step) approach, which requires solving the convection, reaction and diffusion parts of the system separately (see, e.g., [52]), may be inapplicable here. Obviously, the full system (2.1) contains a stabilizing diffusion term, but one has to be very careful since ellipticity of the convective part may still cause instabilities.

We now apply the semi-discrete central-upwind scheme from [32] to (2.2). To this end, we introduce the following notation: $x_\alpha = \alpha \Delta x$, $y_\beta = \beta \Delta y$, where Δx and Δy are small spatial scales assumed, for simplicity, to be constants throughout the computational domain, divided into the cells $C_{j,k} := [x_{j-\frac{1}{2}}, x_{j+\frac{1}{2}}] \times [y_{k-\frac{1}{2}}, y_{k+\frac{1}{2}}]$. According to the central-upwind approach, the cell averages,

$$\overline{\mathbf{U}}_{j,k}(t) := \frac{1}{\Delta x \Delta y} \iint\limits_{C_{j,k}} \mathbf{U}(x, y, t)\, dx dy,$$

are evolved in time by solving the following system of ODEs:

$$\frac{d}{dt}\overline{\mathbf{U}}_{j,k} = -\frac{\mathbf{H}^x_{j+\frac{1}{2},k} - \mathbf{H}^x_{j-\frac{1}{2},k}}{\Delta x} - \frac{\mathbf{H}^y_{j,k+\frac{1}{2}} - \mathbf{H}^y_{j,k-\frac{1}{2}}}{\Delta y}$$

$$+ \Lambda \left[\frac{\overline{\mathbf{U}}_{j+1,k} - 2\overline{\mathbf{U}}_{j,k} + \overline{\mathbf{U}}_{j-1,k}}{(\Delta x)^2} + \frac{\overline{\mathbf{U}}_{j,k+1} - 2\overline{\mathbf{U}}_{j,k} + \overline{\mathbf{U}}_{j,k-1}}{(\Delta y)^2} \right] + \overline{\mathbf{R}}_{j,k}, \quad (2.4)$$

where Λ is a diagonal diffusion matrix (in our case, it is equal to the identity matrix). The numerical fluxes $\mathbf{H}^x$ and $\mathbf{H}^y$ in (2.4) are given by (see [30,32] for details):

$$\mathbf{H}^x_{j+\frac{1}{2},k} = \frac{a^+_{j+\frac{1}{2},k}\mathbf{f}(\mathbf{U}^E_{j,k}) - a^-_{j+\frac{1}{2},k}\mathbf{f}(\mathbf{U}^W_{j+1,k})}{a^+_{j+\frac{1}{2},k} - a^-_{j+\frac{1}{2},k}} + \frac{a^+_{j+\frac{1}{2},k}a^-_{j+\frac{1}{2},k}}{a^+_{j+\frac{1}{2},k} - a^-_{j+\frac{1}{2},k}} \left[\mathbf{U}^W_{j+1,k} - \mathbf{U}^E_{j,k} \right],$$

$$(2.5)$$

$$\mathbf{H}^y_{j,k+\frac{1}{2}} = \frac{b^+_{j,k+\frac{1}{2}}\mathbf{g}(\mathbf{U}^N_{j,k}) - b^-_{j,k+\frac{1}{2}}\mathbf{g}(\mathbf{U}^S_{j,k+1})}{b^+_{j,k+\frac{1}{2}} - b^-_{j,k+\frac{1}{2}}} + \frac{b^+_{j,k+\frac{1}{2}}b^-_{j,k+\frac{1}{2}}}{b^+_{j,k+\frac{1}{2}} - b^-_{j,k+\frac{1}{2}}} \left[\mathbf{U}^S_{j,k+1} - \mathbf{U}^N_{j,k} \right].$$

Here, $\mathbf{U}^{E,W,N,S}_{j,k}$ are the point values of the piecewise linear reconstruction $\widetilde{\mathbf{U}} \equiv (\widetilde{u}, \widetilde{p}, \widetilde{q})$ for $\mathbf{U}$,

$$\widetilde{\mathbf{U}}(x, y) := \overline{\mathbf{U}}_{j,k} + (\mathbf{U}_x)_{j,k}(x - x_j) + (\mathbf{U}_y)_{j,k}(y - y_k), \quad (x, y) \in C_{j,k}, \quad (2.6)$$

at $(x_{j+\frac{1}{2}}, y_k)$, $(x_{j-\frac{1}{2}}, y_k)$, $(x_j, y_{k+\frac{1}{2}})$, and $(x_j, y_{k-\frac{1}{2}})$, respectively. Namely, we have:

$$\begin{aligned} \mathbf{U}^E_{j,k} &:= \widetilde{\mathbf{U}}(x_{j+\frac{1}{2}} - 0, y_k) = \overline{\mathbf{U}}_{j,k} + \frac{\Delta x}{2}(\mathbf{U}_x)_{j,k}, \\ \mathbf{U}^W_{j,k} &:= \widetilde{\mathbf{U}}(x_{j-\frac{1}{2}} + 0, y_k) = \overline{\mathbf{U}}_{j,k} - \frac{\Delta x}{2}(\mathbf{U}_x)_{j,k}, \\ \mathbf{U}^N_{j,k} &:= \widetilde{\mathbf{U}}(x_j, y_{k+\frac{1}{2}} - 0) = \overline{\mathbf{U}}_{j,k} + \frac{\Delta y}{2}(\mathbf{U}_y)_{j,k}, \\ \mathbf{U}^S_{j,k} &:= \widetilde{\mathbf{U}}(x_j, y_{k-\frac{1}{2}} + 0) = \overline{\mathbf{U}}_{j,k} - \frac{\Delta y}{2}(\mathbf{U}_y)_{j,k}. \end{aligned} \quad (2.7)$$

The numerical derivatives $(\mathbf{U}_x)_{j,k}$ and $(\mathbf{U}_y)_{j,k}$ are (at least) first-order approximations of $\mathbf{U}_x(x_j, y_k, t)$ and $\mathbf{U}_y(x_j, y_k, t)$, respectively, and are computed using a nonlinear limiter that would ensure a nonoscillatory nature of the reconstruction (2.6). A library of such limiters is available (see, e.g., [16,28,35–37,42,49]), and one can compute the numerical derivatives using one's favorite limiter. However, it is important that the reconstruction of the cell density, $\widetilde{u}$, is positivity preserving, namely, if $\overline{u}_{j,k} \geq 0 \; \forall j, k$, then the reconstructed point values, $\{u^{E,W,N,S}_{j,k}\}$, are nonnegative as well. In our numerical experiments, we have used the positivity preserving generalized minmod

reconstruction [35,37,42,49] with:

$$
(\mathbf{U}_x)_{j,k} = \mathrm{minmod}\left(\theta\,\frac{\overline{\mathbf{U}}_{j,k} - \overline{\mathbf{U}}_{j-1,k}}{\Delta x},\ \frac{\overline{\mathbf{U}}_{j+1,k} - \overline{\mathbf{U}}_{j-1,k}}{2\Delta x},\ \theta\,\frac{\overline{\mathbf{U}}_{j+1,k} - \overline{\mathbf{U}}_{j,k}}{\Delta x}\right),
$$

$$
(\mathbf{U}_y)_{j,k} = \mathrm{minmod}\left(\theta\,\frac{\overline{\mathbf{U}}_{j,k} - \overline{\mathbf{U}}_{j,k-1}}{\Delta y},\ \frac{\overline{\mathbf{U}}_{j,k+1} - \overline{\mathbf{U}}_{j,k-1}}{2\Delta y},\ \theta\,\frac{\overline{\mathbf{U}}_{j,k+1} - \overline{\mathbf{U}}_{j,k}}{\Delta y}\right),
$$

(2.8)

where the minmod function, defined as

$$
\mathrm{minmod}(z_1, z_2, \ldots) := \begin{cases} \min_j\{z_j\}, & \text{if } z_j > 0 \ \forall j, \\ \max_j\{z_j\}, & \text{if } z_j < 0 \ \forall j, \\ 0, & \text{otherwise}, \end{cases}
$$

is applied in a componentwise manner. The parameter θ can be used to control the amount of numerical viscosity present in the resulting scheme: larger values of θ correspond to less dissipative but, in general, more oscillatory reconstructions.

The one-sided local speeds in the x- and y-directions, $a^{\pm}_{j+\frac{1}{2},k}$ and $b^{\pm}_{j,k+\frac{1}{2}}$, are determined as follows. If all the eigenvalues of the Jacobian $\frac{\partial \mathbf{f}}{\partial \mathbf{U}}$ are real (i.e., if both $\chi(p^{E}_{j,k})^2 \geq 4u^{E}_{j,k}$ and $\chi(p^{W}_{j+1,k})^2 \geq 4u^{W}_{j+1,k}$), then $a^{\pm}_{j+\frac{1}{2},k}$ are obtained from the largest and the smallest eigenvalues of the Jacobian (see (2.3)):

$$
a^{+}_{j+\frac{1}{2},k} = \frac{\chi}{2}\max\left(p^{E}_{j,k} + \sqrt{(p^{E}_{j,k})^2 - \frac{4u^{E}_{j,k}}{\chi}},\ p^{W}_{j+1,k} + \sqrt{(p^{W}_{j+1,k})^2 - \frac{4u^{W}_{j+1,k}}{\chi}},\ 0\right),
$$

$$
a^{-}_{j+\frac{1}{2},k} = \frac{\chi}{2}\min\left(p^{E}_{j,k} - \sqrt{(p^{E}_{j,k})^2 - \frac{4u^{E}_{j,k}}{\chi}},\ p^{W}_{j+1,k} - \sqrt{(p^{W}_{j+1,k})^2 - \frac{4u^{W}_{j+1,k}}{\chi}},\ 0\right),
$$

(2.9)

otherwise we take $a^{\pm}_{j+\frac{1}{2},k}$ to be:

$$
a^{+}_{j+\frac{1}{2},k} = \chi\max\left(p^{E}_{j,k},\ p^{W}_{j+1,k},\ 0\right),\qquad a^{-}_{j+\frac{1}{2},k} = \chi\min\left(p^{E}_{j,k},\ p^{W}_{j+1,k},\ 0\right). \quad (2.10)
$$

In fact, in the elliptic region, the propagation speeds are infinite. However, the values of $a^{\pm}_{j+\frac{1}{2},k}$ chosen in (2.10) guarantee positivity of the computed cell densities as we show in Sect. 2.1.

The y-propagation speeds are computed in a similar fashion: if both $\chi(q^{N}_{j,k})^2 \geq 4u^{N}_{j,k}$ and $\chi(q^{S}_{j,k+1})^2 \geq 4u^{S}_{j,k+1}$, then $b^{\pm}_{j,k+\frac{1}{2}}$ are obtained from the largest and the

smallest eigenvalues of the Jacobian $\frac{\partial \mathbf{g}}{\partial \mathbf{U}}$ (see (2.3)):

$$
b^+_{j,k+\frac{1}{2}} = \frac{\chi}{2} \max \left(q^N_{j,k} + \sqrt{(q^N_{j,k})^2 - \frac{4u^N_{j,k}}{\chi}}, \ q^S_{j,k+1} + \sqrt{(q^S_{j,k+1})^2 - \frac{4u^S_{j,k+1}}{\chi}}, \ 0 \right),
$$

$$
(2.11)
$$

$$
b^-_{j,k+\frac{1}{2}} = \frac{\chi}{2} \min \left(q^N_{j,k} - \sqrt{(q^N_{j,k})^2 - \frac{4u^N_{j,k}}{\chi}}, \ q^S_{j,k+1} - \sqrt{(q^S_{j,k+1})^2 - \frac{4u^S_{j,k+1}}{\chi}}, \ 0 \right),
$$

otherwise we take:

$$
b^+_{j,k+\frac{1}{2}} = \chi \max \left(q^N_{j,k}, \ q^S_{j,k+1}, \ 0 \right), \quad b^-_{j,k+\frac{1}{2}} = \chi \min \left(q^N_{j,k}, \ q^S_{j,k+1}, \ 0 \right). \quad (2.12)
$$

The cell averages of the reaction terms, $\{\overline{\mathbf{R}}_{j,k}\}$, in (2.4) are computed using the midpoint rule, namely:

$$
\overline{R}^{(1)}_{j,k} = 0, \quad \overline{R}^{(2)}_{j,k} = -\overline{p}_{j,k}, \quad \overline{R}^{(3)}_{j,k} = -\overline{q}_{j,k}, \quad (2.13)
$$

where $\mathbf{R} = (R^{(1)}, R^{(2)}, R^{(3)})^T$.

Notice, that in Eqs. (2.4)–(2.13), we suppress the dependence of $\overline{\mathbf{U}}_{j,k}$, $\mathbf{H}^x_{j+\frac{1}{2},k}$, $\mathbf{H}^y_{j,k+\frac{1}{2}}$, $\overline{\mathbf{R}}_{j,k}$, $\mathbf{U}^{E,W,N,S}_{j,k}$, $(\mathbf{U}_x)_{j,k}$, $(\mathbf{U}_y)_{j,k}$, $a^\pm_{j+\frac{1}{2},k}$, and $b^\pm_{j,k+\frac{1}{2}}$ on t to simplify the notation.

Remark Since the third component of the **f** flux and the second component of the **g** flux are zero, the amount of numerical diffusion present at the central-upwind scheme (2.4)–(2.7), (2.9)–(2.13) can be safely decreased by taking $(H^x)^{(3)}_{j+\frac{1}{2},k} \equiv 0$ and $(H^y)^{(2)}_{j,k+\frac{1}{2}} \equiv 0$ for all j, k, where $\mathbf{H} = (H^{(1)}, H^{(2)}, H^{(3)})^T$. This has been done in all numerical experiments reported in Sect. 3.1.

Finally, the system of ODEs (2.4) has to be numerically solved by a sufficiently accurate and stable ODE solver. Since the system (2.4) is rather stiff, one may prefer to use an implicit or large stability domain explicit ODE solver. However, this may affect the positivity preserving property of the resulting fully discrete scheme. In Sect. 2.1, we prove that if one uses the forward Euler method or another strong stability preserving (SSP) method (either the Runge–Kutta or a multistep one) from [18], then the positivity of u will be ensured. The SSP methods are not very efficient for stiff problems. Therefore, it is worthwhile to implement an adaptive strategy by switching between a highly efficient, but not positivity preserving ODE solver, and the SSP method in the following manner. The efficient ODE solver is used from the beginning. If after a certain time step, a negative value of the computed cell density emerges, this step should be rejected and an SSP time step should be performed instead. Then, one has to switch back to the efficient solver.

2.1 Proof of the positivity preserving property

Theorem 2.1 *Consider the system* (2.2) *and the semi-discrete central-upwind scheme* (2.4)–(2.7), (2.9)–(2.13) *with a positivity preserving piecewise linear reconstruction for u. Assume that the system of ODEs* (2.4) *is discretized by the forward Euler method. Then, the computed cell densities* $\{\overline{u}_{j,k}(t)\}$ *remain nonnegative provided the initial cell densities are nonnegative and the following CFL condition is satisfied:*

$$\Delta t \le \min\left\{\frac{\Delta x}{8a}, \frac{\Delta y}{8b}, \frac{(\Delta x)^2(\Delta y)^2}{4((\Delta x)^2+(\Delta y)^2)}\right\}. \tag{2.14}$$

where

$$a := \max_{j,k}\left\{\max\left\{a^+_{j+\frac{1}{2},k}, -a^-_{j+\frac{1}{2},k}\right\}\right\}, \quad b := \max_{j,k}\left\{\max\left\{b^+_{j,k+\frac{1}{2}}, -b^-_{j,k+\frac{1}{2}}\right\}\right\}. \tag{2.15}$$

Proof The proof of this theorem is a straightforward extension of the proof of the positivity preserving property of central-upwind schemes for the Saint–Venant system of shallow water equations [30,33] (see also [32,34]).

Let us assume that at a certain time level t the computed solution is available and that $\overline{u}_{j,k}(t) \ge 0 \,\forall j, k$. Then the new cell densities are obtained from the forward Euler discretization of the first equation in (2.4):

$$\overline{u}_{j,k}(t+\Delta t) = \overline{u}_{j,k} - \lambda\left((H^x)^{(1)}_{j+\frac{1}{2},k} - (H^x)^{(1)}_{j-\frac{1}{2},k}\right) - \mu\left((H^y)^{(1)}_{j,k+\frac{1}{2}} - (H^y)^{(1)}_{j,k-\frac{1}{2}}\right)$$

$$+ \Delta t\left[\frac{\overline{u}_{j+1,k} - 2\overline{u}_{j,k} + \overline{u}_{j-1,k}}{(\Delta x)^2} + \frac{\overline{u}_{j,k+1} - 2\overline{u}_{j,k} + \overline{u}_{j,k-1}}{(\Delta y)^2}\right], \tag{2.16}$$

where $\lambda := \Delta t/\Delta x$, $\mu := \Delta t/\Delta y$, and, as before, the dependence of all terms on the RHS of (2.16) on t is suppressed to simplify the notation. Since

$$(H^x)^{(1)}_{j+\frac{1}{2},k} = \chi \frac{a^+_{j+\frac{1}{2},k} u^E_{j,k} p^E_{j,k} - a^-_{j+\frac{1}{2},k} u^W_{j+1,k} p^W_{j+1,k}}{a^+_{j+\frac{1}{2},k} - a^-_{j+\frac{1}{2},k}}$$

$$+ \frac{a^+_{j+\frac{1}{2},k} a^-_{j+\frac{1}{2},k}}{a^+_{j+\frac{1}{2},k} - a^-_{j+\frac{1}{2},k}}\left[u^W_{j+1,k} - u^E_{j,k}\right]$$

and

$$(H^y)^{(1)}_{j,k+\frac{1}{2}} = \chi \frac{b^+_{j,k+\frac{1}{2}} u^N_{j,k} q^N_{j,k} - b^-_{j,k+\frac{1}{2}} u^S_{j,k+1} q^S_{j,k+1}}{b^+_{j,k+\frac{1}{2}} - b^-_{j,k+\frac{1}{2}}}$$

$$+ \frac{b^+_{j,k+\frac{1}{2}} b^-_{j,k+\frac{1}{2}}}{b^+_{j,k+\frac{1}{2}} - b^-_{j,k+\frac{1}{2}}}\left[u^S_{j,k+1} - u^N_{j,k}\right],$$

and since by the conservation property of the piecewise reconstruction (2.6)

$$\overline{u}_{j,k} = \frac{1}{4}\left(u_{j,k}^{E} + u_{j,k}^{W} + u_{j,k}^{N} + u_{j,k}^{S}\right),$$

which can be rewritten as

$$\overline{u}_{j,k} = \frac{1}{8}\left(u_{j,k}^{E} + u_{j,k}^{W} + u_{j,k}^{N} + u_{j,k}^{S}\right) + \frac{1}{2}\overline{u}_{j,k}, \tag{2.17}$$

we obtain:

$$\overline{u}_{j,k}(t + \Delta t) = \left[\frac{1}{8} + \lambda a_{j-\frac{1}{2},k}^{-}\left(\frac{a_{j-\frac{1}{2},k}^{+} - p_{j,k}^{W}}{a_{j-\frac{1}{2},k}^{+} - a_{j-\frac{1}{2},k}^{-}}\right)\right]u_{j,k}^{W}$$

$$+ \left[\frac{1}{8} - \lambda a_{j+\frac{1}{2},k}^{+}\left(\frac{p_{j,k}^{E} - a_{j+\frac{1}{2},k}^{-}}{a_{j+\frac{1}{2},k}^{+} - a_{j+\frac{1}{2},k}^{-}}\right)\right]u_{j,k}^{E}$$

$$- \lambda a_{j+\frac{1}{2},k}^{-}\left(\frac{a_{j+\frac{1}{2},k}^{+} - p_{j+1,k}^{W}}{a_{j+\frac{1}{2},k}^{+} - a_{j+\frac{1}{2},k}^{-}}\right)u_{j+1,k}^{W}$$

$$+ \lambda a_{j-\frac{1}{2},k}^{+}\left(\frac{p_{j-1,k}^{E} - a_{j-\frac{1}{2},k}^{-}}{a_{j-\frac{1}{2},k}^{+} - a_{j-\frac{1}{2},k}^{-}}\right)u_{j-1,k}^{E}$$

$$+ \left[\frac{1}{8} + \mu b_{j,k-\frac{1}{2}}^{-}\left(\frac{b_{j,k-\frac{1}{2}}^{+} - q_{j,k}^{S}}{b_{j,k-\frac{1}{2}}^{+} - b_{j,k-\frac{1}{2}}^{-}}\right)\right]u_{j,k}^{S}$$

$$+ \left[\frac{1}{8} - \mu b_{j,k+\frac{1}{2}}^{+}\left(\frac{q_{j,k}^{N} - b_{j,k+\frac{1}{2}}^{-}}{b_{j,k+\frac{1}{2}}^{+} - b_{j,k+\frac{1}{2}}^{-}}\right)\right]u_{j,k}^{N}$$

$$- \mu b_{j,k+\frac{1}{2}}^{-}\left(\frac{b_{j,k+\frac{1}{2}}^{+} - q_{j,k+1}^{S}}{b_{j,k+\frac{1}{2}}^{+} - b_{j,k+\frac{1}{2}}^{-}}\right)u_{j,k+1}^{S}$$

$$+ \mu b_{j,k-\frac{1}{2}}^{+}\left(\frac{q_{j,k-1}^{N} - b_{j,k-\frac{1}{2}}^{-}}{b_{j,k-\frac{1}{2}}^{+} - b_{j,k-\frac{1}{2}}^{-}}\right)u_{j,k-1}^{N}$$

$$+ \overline{u}_{j,k}\left[\frac{1}{2} - \Delta t\left(\frac{2}{(\Delta x)^2} + \frac{2}{(\Delta y)^2}\right)\right]$$

$$+ \Delta t\left[\frac{\overline{u}_{j+1,k} + \overline{u}_{j-1,k}}{(\Delta x)^2} + \frac{\overline{u}_{j,k+1} + \overline{u}_{j,k-1}}{(\Delta y)^2}\right]. \tag{2.18}$$

Notice that the new values $\{\overline{u}_{j,k}(t + \Delta t)\}$, computed using (2.18), are linear combinations of the nonnegative reconstructed point value $\{u_{j,k}^{E}, u_{j,k}^{W}, u_{j,k}^{N}, u_{j,k}^{S}\}$ and the

nonnegative cell averages $\{\overline{u}_{j,k}\}$. Moreover, our selection of the local speeds $a^{\pm}_{j+\frac{1}{2},k}$ and $b^{\pm}_{j,k+\frac{1}{2}}$ in (2.9)–(2.12) together with the CFL condition (2.14) guarantees that the coefficients in these linear combinations are nonnegative. Therefore, the new values of the cell densities, computed at time level $t + \Delta t$, are nonnegative. This completes the proof of the theorem.   □

Remarks

1. Notice that one can improve the CFL condition (2.14) by rewriting (2.17) in a more general, one-parameter form:

$$\overline{u}_{j,k} = \frac{\omega}{4}\left(u^{\mathrm{E}}_{j,k} + u^{\mathrm{W}}_{j,k} + u^{\mathrm{N}}_{j,k} + u^{\mathrm{S}}_{j,k}\right) + (1 - \omega)\overline{u}_{j,k}, \quad \omega \in (0, 1).$$

   This would lead to the following estimate:

$$\Delta t \leq \max_{\omega \in (0,1)} \min \left\{ \frac{\omega \Delta x}{4a}, \frac{\omega \Delta y}{4b}, \frac{(1 - \omega)(\Delta x)^2 (\Delta y)^2}{2((\Delta x)^2 + (\Delta y)^2)} \right\},$$

   which is the optimal theoretical CFL condition, but is hard to implement in practice.
2. Theorem 2.1 is also valid if the forward Euler method is replaced by a higher-order SSP ODE solver, because a time step in such solvers can be written as a convex combination of several forward Euler steps.
3. The upper bound on the time step in (2.18) is a minimum of three terms: the first two, $\Delta x/(8a)$ and $\Delta y/(8b)$, are related to the chemotaxis term in the first equation in (2.1), while the third one is due to the parabolic term there. In the (near) blowup regime, a and b in (2.18) are large and thus the first two terms determine the size of time steps, in which case an explicit method is efficient enough. However, when a and b are small, the third term in (2.18) dominates, which reduces the efficiency of the explicit method. One of the ways to overcome this difficulty is to use implicit-explicit (IMEX) methods [3,4,24] as long as a and b remain relatively small. This does not affect the positivity preserving property of our method as we proof in the next theorem.

Theorem 2.2 *Consider the system* (2.2) *and the semi-discrete central-upwind scheme* (2.4)–(2.7), (2.9)–(2.13) *with a positivity preserving piecewise linear reconstruction for u. Assume that the system of ODEs* (2.4) *is discretized by the first-order IMEX method, namely,*

$$\overline{\mathbf{U}}_{j,k}(t + \Delta t) = \overline{\mathbf{U}}_{j,k}(t) - \lambda \left((H^x)^{(1)}_{j+\frac{1}{2},k}(t) - (H^x)^{(1)}_{j-\frac{1}{2},k}(t)\right)$$

$$- \mu \left((H^y)^{(1)}_{j,k+\frac{1}{2}}(t) - (H^y)^{(1)}_{j,k-\frac{1}{2}}(t)\right)$$

$$+ \Delta t \frac{\overline{\mathbf{U}}_{j+1,k}(t + \Delta t) - 2\overline{\mathbf{U}}_{j,k}(t + \Delta t) + \overline{\mathbf{U}}_{j-1,k}(t + \Delta t)}{(\Delta x)^2}$$

$$+ \Delta t \frac{\overline{\mathbf{U}}_{j,k+1}(t + \Delta t) - 2\overline{\mathbf{U}}_{j,k}(t + \Delta t) + \overline{\mathbf{U}}_{j,k-1}(t + \Delta t)}{(\Delta y)^2}$$

$$+ \Delta t \overline{\mathbf{R}}_{j,k}(t + \Delta t). \tag{2.19}$$

Then, the computed cell densities $\{\overline{u}_{j,k}(t)\}$ remain nonnegative provided the initial cell densities are nonnegative and the following CFL condition is satisfied:

$$\Delta t \leq \min\left\{\frac{\Delta x}{4a}, \frac{\Delta y}{4b}\right\}, \tag{2.20}$$

where a and b are give by (2.15).

Proof We begin in exactly the same way as in the proof of Theorem 2.1 and group the terms in the first equation in (2.19) as

$$\overline{u}_{j,k}(t + \Delta t) = \left[\frac{1}{4} + \lambda a^-_{j-\frac{1}{2},k}\left(\frac{a^+_{j-\frac{1}{2},k} - p^{\mathrm{W}}_{j,k}}{a^+_{j-\frac{1}{2},k} - a^-_{j-\frac{1}{2},k}}\right)\right]u^{\mathrm{W}}_{j,k}$$

$$+ \left[\frac{1}{4} - \lambda a^+_{j+\frac{1}{2},k}\left(\frac{p^{\mathrm{E}}_{j,k} - a^-_{j+\frac{1}{2},k}}{a^+_{j+\frac{1}{2},k} - a^-_{j+\frac{1}{2},k}}\right)\right]u^{\mathrm{E}}_{j,k}$$

$$- \lambda a^-_{j+\frac{1}{2},k}\left(\frac{a^+_{j+\frac{1}{2},k} - p^{\mathrm{W}}_{j+1,k}}{a^+_{j+\frac{1}{2},k} - a^-_{j+\frac{1}{2},k}}\right)u^{\mathrm{W}}_{j+1,k}$$

$$+ \lambda a^+_{j-\frac{1}{2},k}\left(\frac{p^{\mathrm{E}}_{j-1,k} - a^-_{j-\frac{1}{2},k}}{a^+_{j-\frac{1}{2},k} - a^-_{j-\frac{1}{2},k}}\right)u^{\mathrm{E}}_{j-1,k}$$

$$+ \left[\frac{1}{4} + \mu b^-_{j,k-\frac{1}{2}}\left(\frac{b^+_{j,k-\frac{1}{2}} - q^{\mathrm{S}}_{j,k}}{b^+_{j,k-\frac{1}{2}} - b^-_{j,k-\frac{1}{2}}}\right)\right]u^{\mathrm{S}}_{j,k}$$

$$+ \left[\frac{1}{4} - \mu b^+_{j,k+\frac{1}{2}}\left(\frac{q^{\mathrm{N}}_{j,k} - b^-_{j,k+\frac{1}{2}}}{b^+_{j,k+\frac{1}{2}} - b^-_{j,k+\frac{1}{2}}}\right)\right]u^{\mathrm{N}}_{j,k}$$

$$- \mu b^-_{j,k+\frac{1}{2}}\left(\frac{b^+_{j,k+\frac{1}{2}} - q^{\mathrm{S}}_{j,k+1}}{b^+_{j,k+\frac{1}{2}} - b^-_{j,k+\frac{1}{2}}}\right)u^{\mathrm{S}}_{j,k+1}$$

$$+ \mu b^+_{j,k-\frac{1}{2}}\left(\frac{q^{\mathrm{N}}_{j,k-1} - b^-_{j,k-\frac{1}{2}}}{b^+_{j,k-\frac{1}{2}} - b^-_{j,k-\frac{1}{2}}}\right)u^{\mathrm{N}}_{j,k-1}$$

$$+ \Delta t \frac{\overline{u}_{j+1,k}(t + \Delta t) - 2\overline{u}_{j,k}(t + \Delta t) + \overline{u}_{j-1,k}(t + \Delta t)}{(\Delta x)^2}$$

$$+ \Delta t \frac{\overline{u}_{j,k+1}(t + \Delta t) - 2\overline{u}_{j,k}(t + \Delta t) + \overline{u}_{j,k-1}(t + \Delta t)}{(\Delta y)^2}. \tag{2.21}$$

(compare with (2.18)). Once again, the time dependence of all terms in (2.21) calculated at time level t is suppressed to simplify the notation.

Next, we rewrite Eq. (2.21) in the following vector form:

$$(I + \Delta t M)\vec{u}(t + \Delta t) = \vec{\mathcal{L}}\left(\vec{u}^{\text{E}}, \vec{u}^{\text{W}}, \vec{u}^{\text{N}}, \vec{u}^{\text{S}}\right), \tag{2.22}$$

where M is a so-called M-matrix [24], $\vec{u}$ is a vector containing the cell averages $\overline{u}_{j,k}(t + \Delta t)$ and $\vec{\mathcal{L}}$ is a vector, each element of which is a linear combination of the corresponding point values $\overline{u}_{j,k}^{\text{E,W,N,S}}$ with the coefficients that are nonnegative provided the CFL condition (2.20) is satisfied. Since all the point values $\overline{u}_{j,k}^{\text{E,W,N,S}}$ are nonnegative, each entry of $\vec{\mathcal{L}}$ is nonnegative as well.

It is well-known [24,47] that all components of the solution of the linear system (2.22),

$$\vec{u}(t + \Delta t) = (I + \Delta t M)^{-1}\vec{\mathcal{L}}\left(\vec{u}^{\text{E}}, \vec{u}^{\text{W}}, \vec{u}^{\text{N}}, \vec{u}^{\text{S}}\right),$$

are also nonnegative. Thus, the proof of the theorem is complete. □

Remark Theorem 2.2 is also valid if the first-order IMEX method is replaced with a high-order IMEX-SSP [43] or a positivity preserving IMEX [20] method.

3 Numerical examples and applications

In this section, we demonstrate the performance of the proposed central-upwind scheme on a number of test problems for the Keller–Segel system. We also show that a naïve finite-difference scheme, described in Sect. 3.1 below, fails to capture solutions of these problems. In addition, we apply our new method to two related problems—two more complicated chemotaxis systems (Sects. 3.2 and 3.3) and the haptotaxis model (Sect. 3.4).

In all numerical examples, we have used the Neumann boundary conditions implemented in a straightforward "zero flux" manner. The central-upwind scheme has always been used with the minmod limiter (2.8) with $\theta = 2$ and the third-order SSP Runge–Kutta ODE solver from [18] for the time evolution. The time step has been selected adaptively according to (2.14).

The efficiency of the proposed central-upwind scheme can be improved by replacing the SSP Runge–Kutta ODE solver with either an IMEX method (see, e.g., [3,4,20, 43]) or by implementing an adaptive switching between a highly efficient (but not necessarily positivity preserving) ODE solver and an explicit SSP method.

3.1 Keller–Segel model

We begin with writing down a finite-difference scheme for the Keller–Segel system (1.1) and (1.2). In the semi-discrete flux form, the scheme reads:

$$
\begin{cases}
\dfrac{du_{j,k}}{dt} = -\dfrac{H^x_{j+\frac{1}{2},k}(t)-H^x_{j-\frac{1}{2},k}(t)}{\Delta x} - \dfrac{H^y_{j,k+\frac{1}{2}}(t)-H^y_{j,k-\frac{1}{2}}(t)}{\Delta y} + \dfrac{u_{j+1,k}(t)-2u_{j,k}(t)+u_{j-1,k}(t)}{(\Delta x)^2} \\
\qquad + \dfrac{u_{j,k+1}(t)-2u_{j,k}(t)+u_{j,k-1}(t)}{(\Delta y)^2}, \\
\dfrac{dv_{j,k}}{dt} = \dfrac{v_{j+1,k}(t)-2v_{j,k}(t)+v_{j-1,k}(t)}{(\Delta x)^2} + \dfrac{v_{j,k+1}(t)-2v_{j,k}(t)+v_{j,k-1}(t)}{(\Delta y)^2} - v_{j,k}(t)+u_{j,k}(t),
\end{cases}
$$
$$(3.1)$$

where $u_{j,k}(t)$ and $v_{j,k}(t)$ denote the approximation of the point values $u(x_j, y_k, t)$ and $v(x_j, y_k, t)$, respectively, and the centered fluxes are:

$$
\begin{aligned}
H^x_{j+\frac{1}{2},k}(t) &= \chi \frac{u_{j+1,k}(t) + u_{j,k}(t)}{2} \cdot \frac{v_{j+1,k}(t) - v_{j,k}(t)}{\Delta x}, \\
H^y_{j,k+\frac{1}{2}}(t) &= \chi \frac{u_{j,k+1}(t) + u_{j,k}(t)}{2} \cdot \frac{v_{j,k+1}(t) - v_{j,k}(t)}{\Delta y}.
\end{aligned}
$$
$$(3.2)$$

The fully discrete finite-difference scheme is then obtained by applying an ODE solver to (3.1) and (3.2). In our numerical experiments, we have tested different ODE solvers and the obtained results did not depend on a particular choice of the time discretization.

Example 1 (Blowup at the center of a square domain. Nonzero $v(x, y, 0)$.) We first consider the initial-boundary value problem (IBVP) for the Keller–Segel system with the chemotactic sensitivity constant $\chi = 1$ and the radially symmetric bell-shaped initial data,

$$
u(x, y, 0) = 1000\, e^{-100(x^2+y^2)}, \quad v(x, y, 0) = 500\, e^{-50(x^2+y^2)}, \tag{3.3}
$$

in a square domain $\left[-\frac{1}{2}, \frac{1}{2}\right] \times \left[-\frac{1}{2}, \frac{1}{2}\right]$.

According to the results in [19], both u- and v-components of the solution are expected to blow up at the origin in finite time. This situation is especially challenging since capturing blowing up solutions with shrinking support is extremely hard.

We first apply the finite-difference scheme (3.1) and (3.2) to the IBVP (1.1), (1.2), and (3.3). We have used a uniform grid with $\Delta x = \Delta y = 1/101$. The computed cell densities at times $t = 10^{-6}$ and $t = 5 \times 10^{-6}$ are plotted in Fig. 1. As one can see, the method performs reasonably well. However, already at $t = 4.4 \times 10^{-5}$ negative densities appear (see Fig. 2) and this triggers severe numerical instabilities. By time $t = 10^{-4}$, the computed solution is already meaningless as it is shown in Fig. 3.

On the contrary, the proposed central-upwind scheme performs well on this test problem. The results obtained on the same uniform grid with $\Delta x = \Delta y = 1/101$ are plotted in Fig. 4. One may observe a lack of negative values of u (as predicted by Theorem 2.1) or any other numerical instabilities, and a high resolution of the blowing up solution. Numerical convergence of the central-upwind scheme is verified by running the same test on a finer grid with $\Delta x = \Delta y = 1/201$, see Fig. 5. As one can see, the coarse and the fine grid solutions are at a very good agreement at small times ($t = 10^{-6}$ and $t = 5 \times 10^{-6}$). However, they are quite different at a larger time $t = 4.4 \times 10^{-5}$, and especially at $t = 10^{-4}$. Therefore, we further refine the grid and
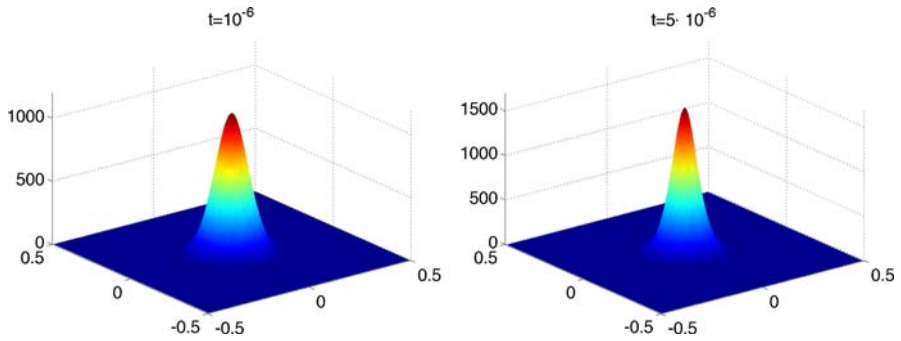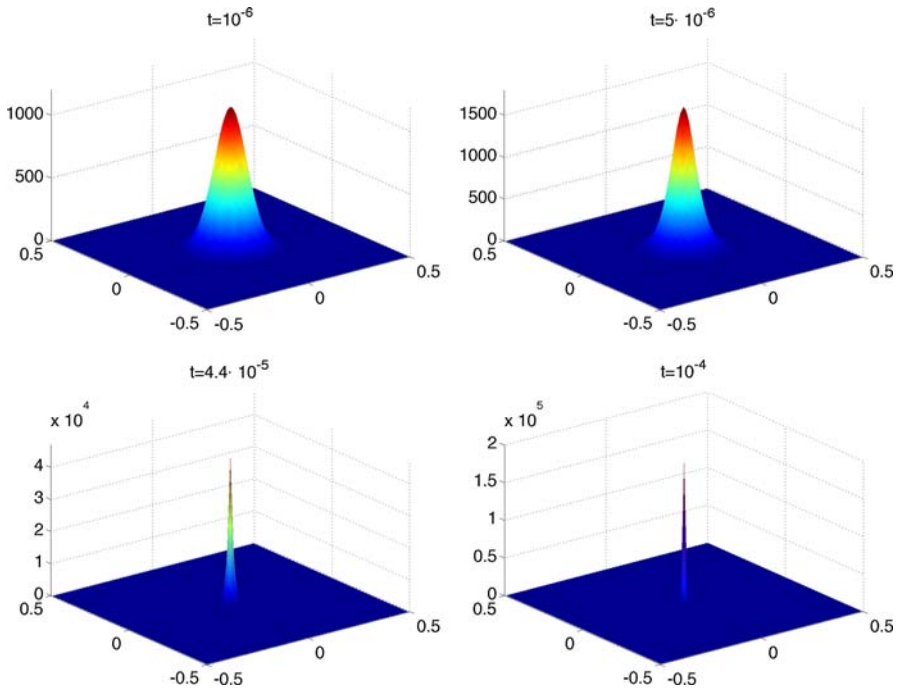
Fig. 1 Solution (u) of (1.1) and (1.2), (3.3) at small times by the finite-difference scheme
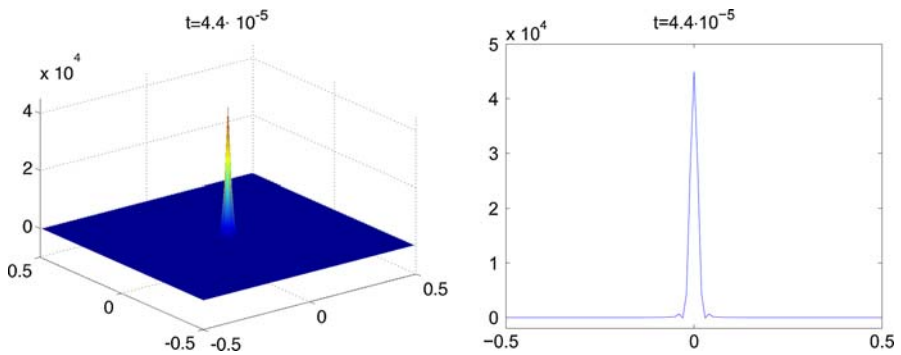
Fig. 2 Solution (u) of (1.1), (1.2), and (3.3) at $t = 4.4 \times 10^{-5}$ by the finite-difference scheme (*left*) and its one-dimensional (1D) slice along $y = 0$ (*right*)
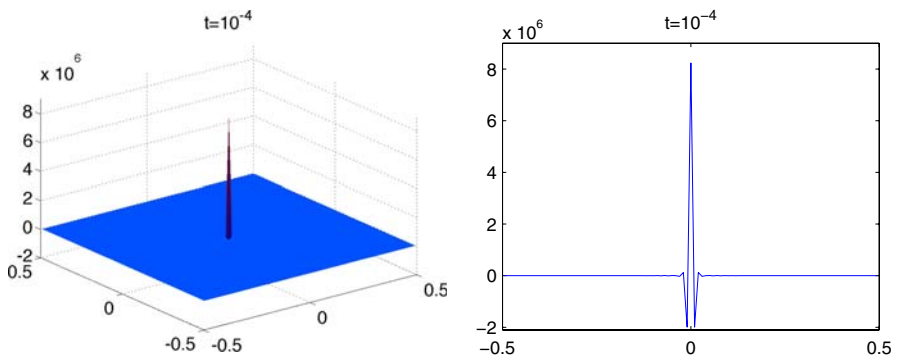
Fig. 3 Solution (u) of (1.1), (1.2), and (3.3) at $t = 10^{-4}$ by the finite-difference scheme (*left*) and its 1D slice along $y = 0$ (*right*)

Fig. 4 Solution (u) of (1.3), (3.3) by the central-upwind scheme with $\Delta x = \Delta y = 1/101$

apply the central-upwind scheme on the uniform grid with $\Delta x = \Delta y = 1/401$ to the same IBVP. The results are shown in Fig. 6. It seems that the computed solution converges at $t = 4.4 \times 10^{-5}$, but it keeps increasing (as the grid is refined) at $t = 10^{-4}$. A more precise interpretation of the obtained results would require a knowledge of the blowup time (which is not available) since after the solution blows up no numerical convergence is expected. Based on the presented numerical results, we conjecture that the blowup time $t^* \in (4.4 \times 10^{-5}, 10^{-4})$.

Figures 4, 5 and 6 clearly demonstrate that the maximum value of u grows in time, while its support shrinks. Since the growth rate is very high, the solutions at different times are plotted in different vertical scales, which makes it somehow inconvenient to visually compare them. It is also quite hard to see details of the computed solution at the blowup stages. Therefore, in Figs. 7, 8 and 9, we plot the same computed solutions, but in the uniform (in time) logarithmic vertical scale. All other results in Sect. 3.1 will be plotted in the logarithmic scale only.

Example 2 Blowup at the center of a square domain. $v(x, y, 0) \equiv 0$ Next, we apply the central-upwind scheme to another IBVP for the same system (1.3) with $\chi = 1$ on the same domain $\left[-\frac{1}{2}, \frac{1}{2}\right] \times \left[-\frac{1}{2}, \frac{1}{2}\right]$, but subject to the different initial data:

$$u(x, y, 0) = 1000 \, e^{-100(x^2 + y^2)}, \quad v(x, y, 0) \equiv 0. \tag{3.4}$$

As in the previous example, both u- and v-components of the solution are expected to blow up at the origin in finite time, [19]. However, the initial chemoattractant
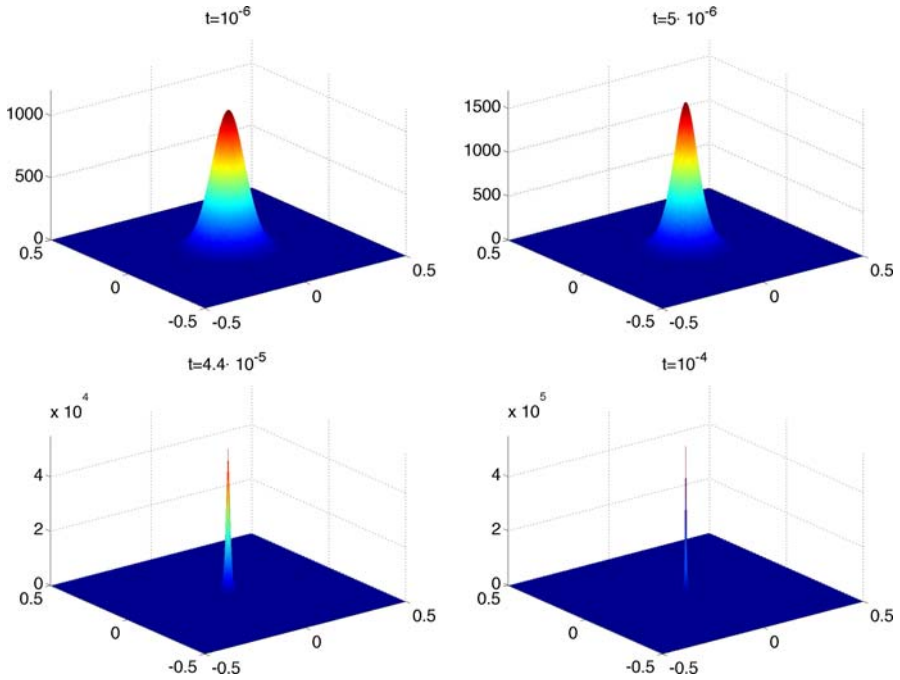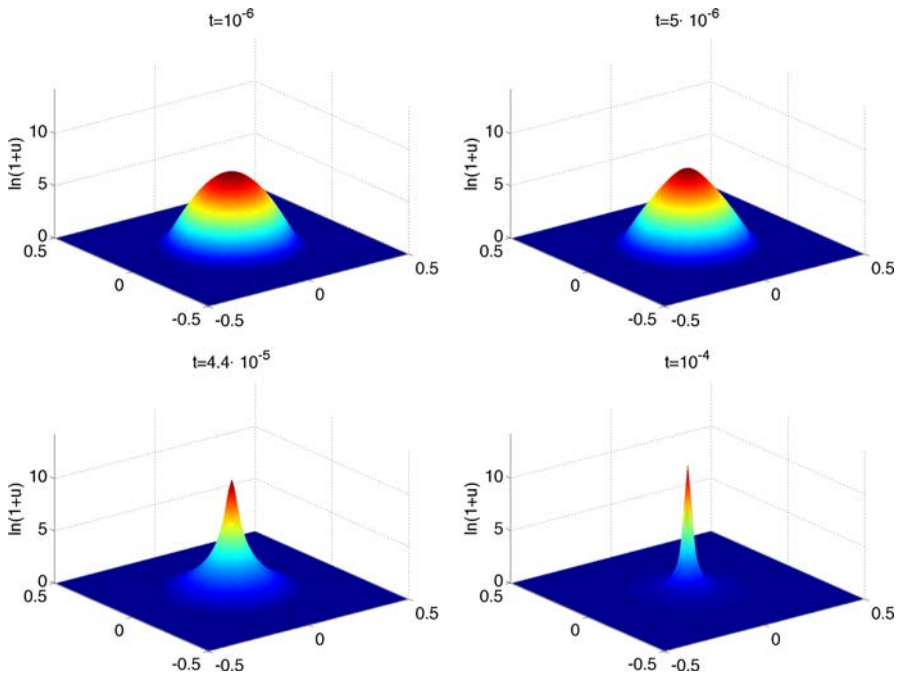
Fig. 5 Same as in Fig. 4 but on a finer grid with $\Delta x = \Delta y = 1/201$
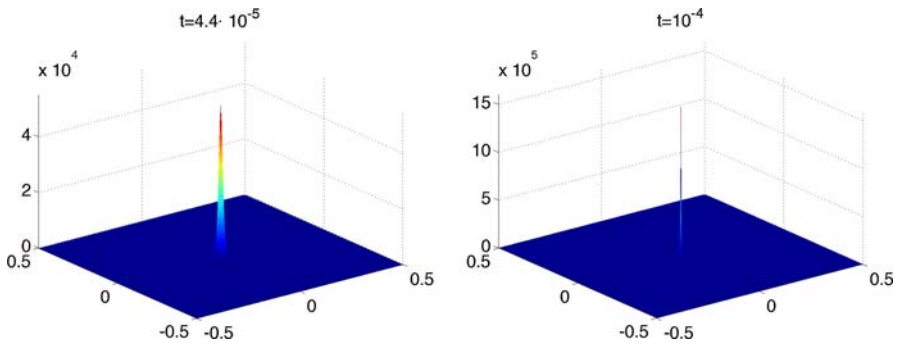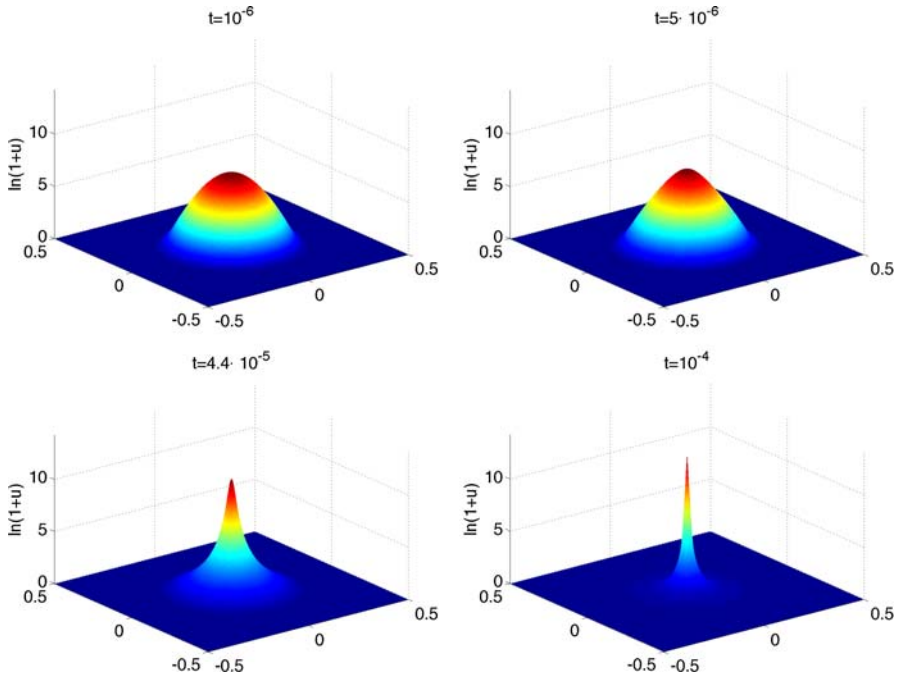

Fig. 6 Same as in Figs. 4 and 5 but on a finer grid with $\Delta x = \Delta y = 1/401$

concentration is now zero, and thus the blowup is expected to occur much later than in Example 1. Moreover, the diffusion initially dominates the concentration mechanism and, as a result, the cell density spreads out and its maximum decreases at small times (the maximum of u, computed at time $t = 0.1$, is $\sim 529.4/541.5$).

The results obtained by the finite-difference scheme (3.1) and (3.2) applied to this IBVP on the uniform grid with $\Delta x = \Delta y = 1/101$ are reasonably good at times $t = 0.1$ and $t = 0.2$, but at about $t \approx 0.31345$ negative cell densities appear, and by time $t = 0.3135$ the computed solution is already meaningless (the numerical
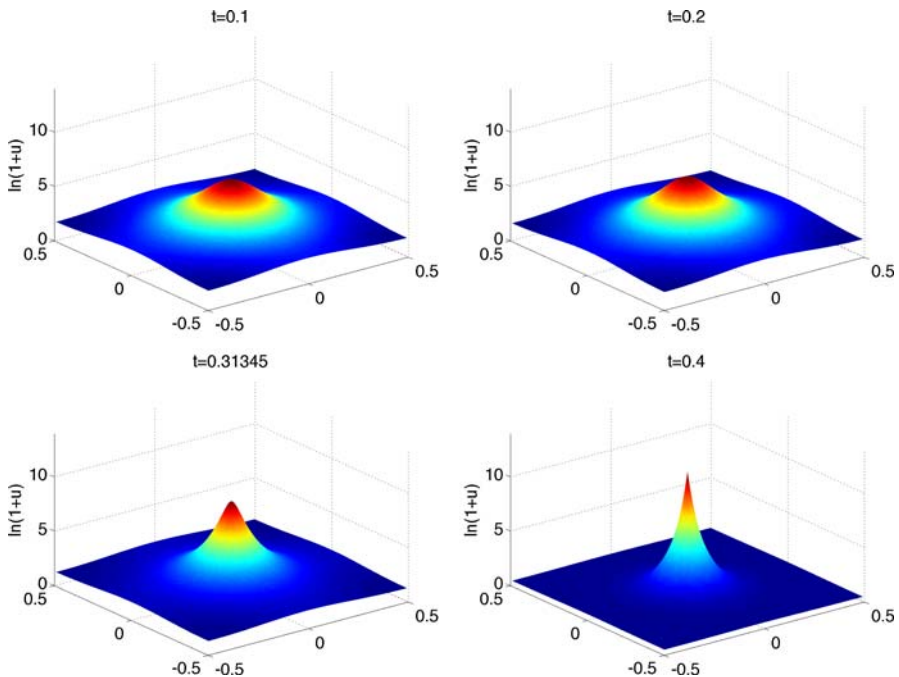
Fig. 7 Solution $(\ln(1 + u))$ of (1.3), (3.3) by the central-upwind scheme with $\Delta x = \Delta y = 1/101$

Fig. 8 Same as in Fig. 7 but on a finer grid with $\Delta x = \Delta y = 1/201$
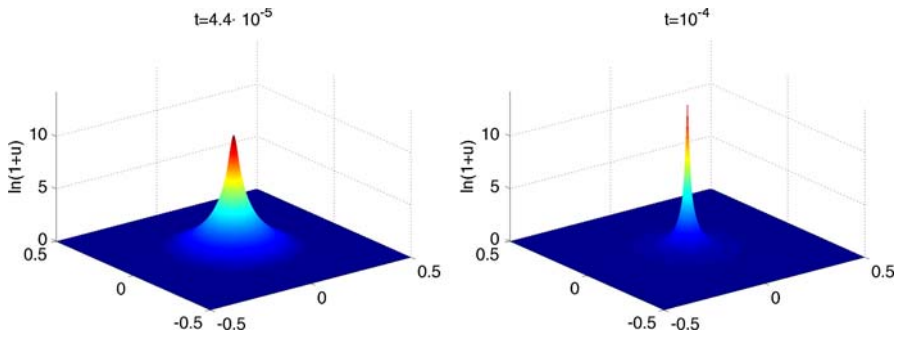
Fig. 9 Same as in Figs. 7 and 8 but on a finer grid with $\Delta x = \Delta y = 1/401$

Fig. 10 Solution $(\ln(1+u))$ of (1.3), (3.4) by the central-upwind scheme with $\Delta x = \Delta y = 1/101$

instability is similar to the one shown in Figs. 2 and 3, so we do not plot any finite-difference results here).

We now apply the central-upwind scheme to this test problem. The results obtained on the same uniform are plotted in Fig. 10. The computed u-component solution has got no negative values and is oscillation-free. Numerical convergence of the central-upwind scheme is verified by running the same test on finer grids with $\Delta x = \Delta y = 1/201$ (Fig. 11) and $\Delta x = \Delta y = 1/401$ (Fig. 12). As in Example 1, no convergence has been observed at the largest shown time ($t = 0.4$). We conjecture that this occurs since $t = 0.4$ is already a post-blowup time.
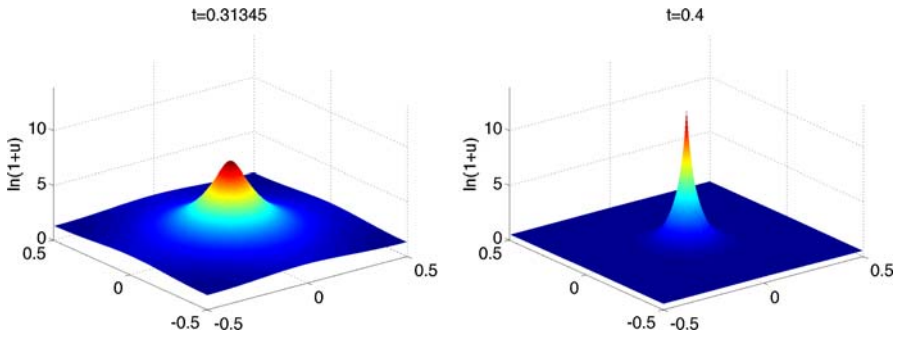
Fig. 11 Same as in Fig. 10 but on a finer grid with $\Delta x = \Delta y = 1/201$
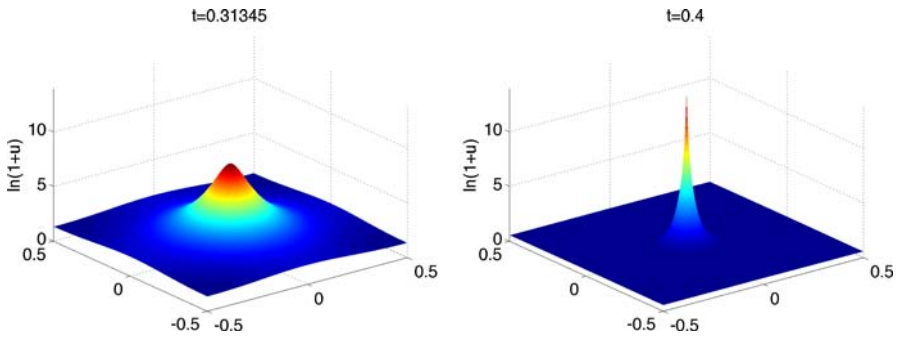

Fig. 12 Same as in Figs. 10 and 11 but on a finer grid with $\Delta x = \Delta y = 1/401$

Example 3 (Blowup at the corner of a square domain.) The third example is designed to demonstrate the ability of the proposed central-upwind scheme to capture solutions that blow up away from their initial location. We consider the same IBVP as in Example 2, but with the initial data shifted by $(0.25, 0.25)$:

$$u(x, y, 0) = 1000e^{-100((x-0.25)^2+((y-0.25)^2)}, \quad v(x, y, 0) = 0. \tag{3.5}$$

It has been proved in [19] that in this case, the solution is expected to blow up at the boundary of the domain. The cell densities computed by the central-upwind scheme at different times on two different uniform grids are shown (in the logarithmic scale) in Figs. 13 and 14. Once again, one may observe that the behavior of the computed solution matches the prediction: the cells first move to the boundary and then concentrate at the corner where the solution blows up.
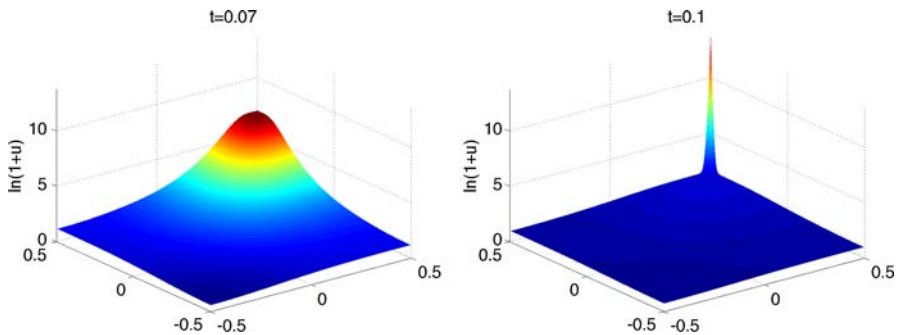
We also consider the same IBVP but with a twice smaller initial cell density:

$$u(x, y, 0) = 500e^{-100((x-0.25)^2+((y-0.25)^2)}, \quad v(x, y, 0) = 0. \tag{3.6}$$

According to [19], the solution of this IBVP is expected to be different form the previous one. The total mass is now below the critical value, and thus the solution
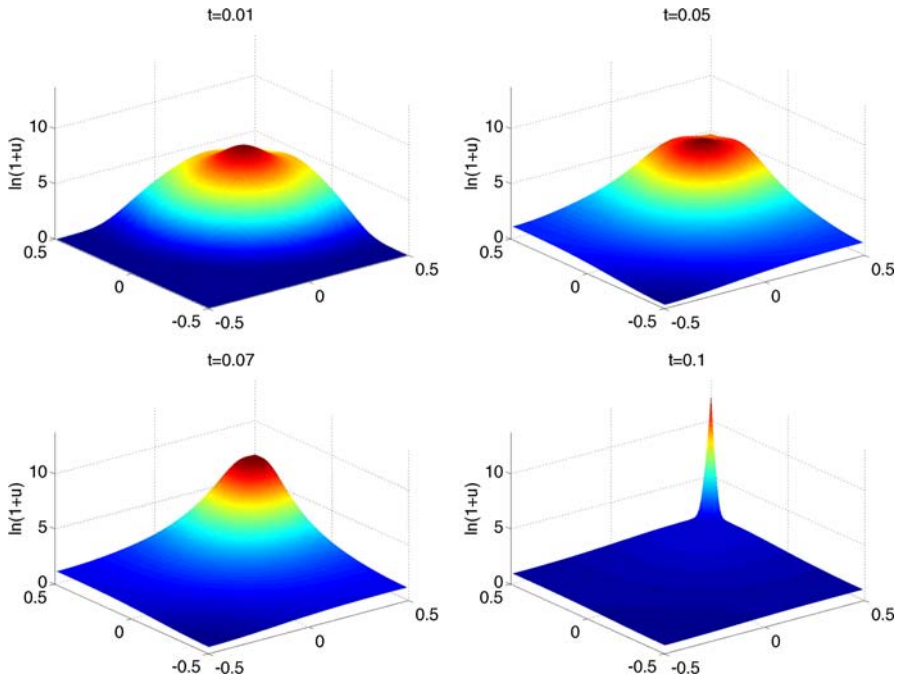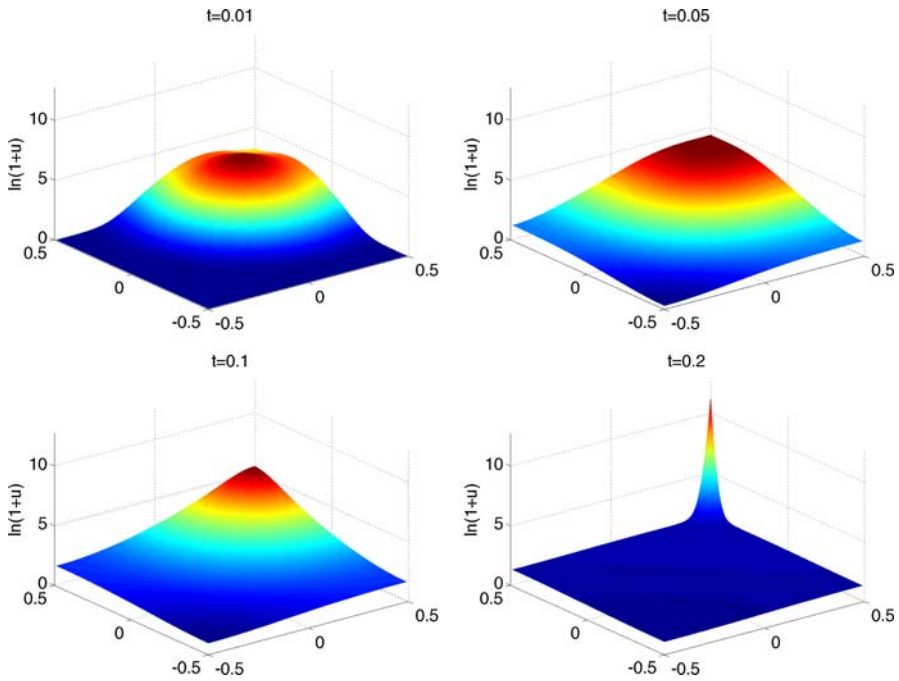
Fig. 13 Solution ($\ln(1 + u)$) of (1.3), (3.5) by the central-upwind scheme with $\Delta x = \Delta y = 1/101$


Fig. 14 Same as in Fig. 13 but on a finer grid with $\Delta x = \Delta y = 1/201$

may or may not blow up, and if it does, it has to concentrate at the boundary of the domain. The cell densities (in the logarithmic scale) computed at different times on two different uniform grids are shown in Figs. 15 and 16. Our results suggest that even though the total mass is below the critical one, the solution still blows up at the corner. However, at the early stages, the solution spreads out over the entire domain and the maximum of u reduces to $\sim 79.35/79.41$ at time $t = 0.05$, and only later on it starts concentrating at the corner. As expected, the entire blowup process takes more time than in the case of the IBVP (1.3), (3.5).

Fig. 15 Solution $(\ln(1 + u))$ of (1.3), (3.6) by the central-upwind scheme with $\Delta x = \Delta y = 1/101$
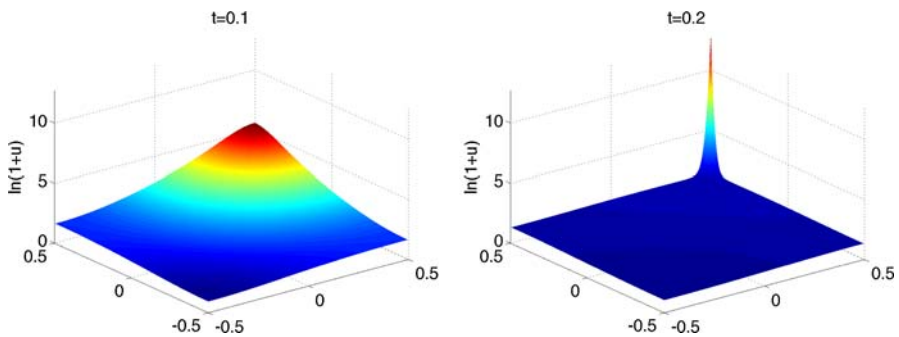
Fig. 16 Same as in Fig. 15 but on a finer grid $\Delta x = \Delta y = 1/201$

3.2 Model of chemotactic bacteria patterns in semi-solid medium

In this section, we consider a more complicated and more realistic chemotaxis model proposed in [51] (see also [52]), which, in dimensionless form, can be written as:

$$u_t + \alpha \nabla \cdot \left[\frac{u}{(1 + v)^2} \nabla v \right] = d_u \Delta u + \rho u \left(\delta \frac{w^2}{1 + w^2} - u \right) \qquad (3.7)$$

$$v_t = d_v \Delta v + \beta \frac{wu^2}{\sigma + u^2} - \gamma uv, \tag{3.8}$$

$$w_t = d_w \Delta w - \kappa u \frac{w^2}{1 + w^2} \tag{3.9}$$

Here, as before, $u(x, y, t)$ and $v(x, y, t)$ are the cell density and a chemoattractant concentration, respectively. The new variable $w(x, y, t)$ represents the nutrient concentration and the coefficients $\alpha, d_u, \rho, \delta, d_v, \beta, \sigma, \gamma, d_w$, and κ are positive constants.

According to our approach described in Sects. 1 and 2, we first differentiate equation (3.8) with respect to x and y, and add two new equations to the system (3.7)–(3.9). We obtain:

$$
\begin{cases}
u_t + \left(\dfrac{\alpha u p}{(1 + v)^2} \right)_x + \left(\dfrac{\alpha u q}{(1 + v)^2} \right)_y = d_u(u_{xx} + u_{yy}) + \rho u \left(\dfrac{\delta w^2}{1 + w^2} - u \right), \\[2ex]
v_t = d_v(v_{xx} + v_{yy}) + \dfrac{\beta w u^2}{\sigma + u^2} - \gamma uv, \\[2ex]
p_t + \left(\gamma uv - \dfrac{\beta w u^2}{\sigma + u^2} \right)_x = d_v(p_{xx} + p_{yy}), \\[2ex]
q_t + \left(\gamma uv - \dfrac{\beta w u^2}{\sigma + u^2} \right)_y = d_v(q_{xx} + q_{yy}), \\[2ex]
w_t = d_w \Delta w - \dfrac{\kappa u w^2}{1 + w^2}
\end{cases}
$$

where, as before, $p := v_x$, $q := v_y$. In the flux form, this system reads:

$$\mathbf{U}_t + \mathbf{f}(\mathbf{U})_x + \mathbf{g}(\mathbf{U})_y = \Lambda(\mathbf{U}_{xx} + \mathbf{U}_{yy}) + \mathbf{R}(\mathbf{U}), \tag{3.10}$$

where $\mathbf{U} := (u, v, p, q, w)^T$, the fluxes are $\mathbf{f}(\mathbf{U}) := \left(\frac{\alpha u p}{(1+v)^2}, 0, \gamma uv - \frac{\beta w u^2}{\sigma + u^2}, 0, 0 \right)^T$ and $\mathbf{g}(\mathbf{U}) := \left(\frac{\alpha u q}{(1+v)^2}, 0, 0, \gamma uv - \frac{\beta w u^2}{\sigma + u^2}, 0 \right)^T$, the diffusion matrix is $\Lambda := \text{diag}(d_u, d_v, d_v, d_v, d_w)$, and the source term is $\mathbf{R}(\mathbf{U}) := \left(\rho u \left(\frac{\delta w^2}{1+w^2} - u \right), \frac{\beta w u^2}{\sigma + u^2} - \gamma uv, 0, 0, -\frac{\kappa u w^2}{1+w^2} \right)^T$. The eigenvalues of the Jacobians $\frac{\partial \mathbf{f}}{\partial \mathbf{U}}$ and $\frac{\partial \mathbf{g}}{\partial \mathbf{U}}$ are:

$$\lambda^{\mathbf{f}}_{1,2} = \frac{\alpha}{2(1 + v)^2} \left(p \pm \sqrt{p^2 - \frac{4u(\gamma v - 2\beta \sigma uw)(1 + v)^2}{\alpha(\sigma + u^2)^2}} \right), \quad \lambda^{\mathbf{f}}_3 = \lambda^{\mathbf{f}}_4 = \lambda^{\mathbf{f}}_5 = 0 \tag{3.11}$$

and

$$\lambda^{\mathbf{g}}_{1,2} = \frac{\alpha}{2(1 + v)^2} \left(q \pm \sqrt{q^2 - \frac{4u(\gamma v - 2\beta \sigma uw)(1 + v)^2}{\alpha(\sigma + u^2)^2}} \right), \quad \lambda^{\mathbf{g}}_3 = \lambda^{\mathbf{g}}_4 = \lambda^{\mathbf{g}}_5 = 0, \tag{3.12}$$

respectively. Since the expression under the square root in (3.11) and (3.12) may be negative, the convective part of the system (3.10) is only conditionally hyperbolic.

The positivity preserving semi-discrete central-upwind scheme for this system is obtained in the same way as for the Keller–Segel system (2.2). The only difference is in the computation of the one-sided local speeds and the cell averages of the reaction term. The x-speeds are now given by:

$$
a_{j+\frac{1}{2},k}^{+} = \frac{\alpha}{2} \max \left(\frac{p_{j,k}^{E}}{(1+v_{j,k}^{E})^2} + \sqrt{\frac{(p_{j,k}^{E})^2}{(1+v_{j,k}^{E})^4} - \frac{4(u_{j,k}^{E})(\gamma v_{j,k}^{E} - 2\beta\sigma u_{j,k}^{E} w_{j,k}^{E})}{\alpha(1+v_{j,k}^{E})^2(\sigma+(u_{j,k}^{E})^2)^2}} \right. ,
$$
$$
\left. \frac{p_{j+1,k}^{W}}{(1+v_{j+1,k}^{W})^2} + \sqrt{\frac{(p_{j+1,k}^{W})^2}{(1+v_{j+1,k}^{W})^4} - \frac{4(u_{j+1,k}^{W})^2(\gamma v_{j+1,k}^{W} - 2\beta\sigma u_{j+1,k}^{W} w_{j+1,k}^{W})}{\alpha(1+v_{j+1,k}^{W})^2(\sigma+(u_{j+1,k}^{W})^2)^2}} , 0 \right),
$$

$$
a_{j+\frac{1}{2},k}^{-} = \frac{\alpha}{2} \min \left(\frac{p_{j,k}^{E}}{(1+v_{j,k}^{E})^2} - \sqrt{\frac{(p_{j,k}^{E})^2}{(1+v_{j,k}^{E})^4} - \frac{4(u_{j,k}^{E})(\gamma v_{j,k}^{E} - 2\beta\sigma u_{j,k}^{E} w_{j,k}^{E})}{\alpha(1+v_{j,k}^{E})^2(\sigma+(u_{j,k}^{E})^2)^2}} \right. ,
$$
$$
\left. \frac{p_{j+1,k}^{W}}{(1+v_{j+1,k}^{W})^2} - \sqrt{\frac{(p_{j+1,k}^{W})^2}{(1+v_{j+1,k}^{W})^4} - \frac{4(u_{j+1,k}^{W})^2(\gamma v_{j+1,k}^{W} - 2\beta\sigma u_{j+1,k}^{W} w_{j+1,k}^{W})}{\alpha(1+v_{j+1,k}^{W})^2(\sigma+(u_{j+1,k}^{W})^2)^2}} , 0 \right),
$$

(3.13)

if all the expressions under the square roots in (3.13) are defined, and

$$
a_{j+\frac{1}{2},k}^{+} = \alpha \max \left(\frac{p_{j,k}^{E}}{(1+v_{j,k}^{E})^2}, \frac{p_{j+1,k}^{W}}{(1+v_{j+1,k}^{W})^2}, 0 \right),
$$

$$
a_{j+\frac{1}{2},k}^{-} = \alpha \min \left(\frac{p_{j,k}^{E}}{(1+v_{j,k}^{E})^2}, \frac{p_{j+1,k}^{W}}{(1+v_{j+1,k}^{W})^2}, 0 \right),
$$

otherwise. The one-sided local speeds in the y-direction are computed similarly:

$$
b_{j,k+\frac{1}{2}}^{+} = \frac{\alpha}{2} \max \left(\frac{q_{j,k}^{N}}{(1+v_{j,k}^{N})^2} + \sqrt{\frac{(q_{j,k}^{N})^2}{(1+v_{j,k}^{N})^4} - \frac{4(u_{j,k}^{N})(\gamma v_{j,k}^{N} - 2\beta\sigma u_{j,k}^{N} w_{j,k}^{N})}{\alpha(1+v_{j,k}^{N})^2(\sigma+(u_{j,k}^{N})^2)^2}} \right. ,
$$
$$
\left. \frac{q_{j,k+1}^{S}}{(1+v_{j,k+1}^{S})^2} + \sqrt{\frac{(q_{j,k+1}^{S})^2}{(1+v_{j,k+1}^{S})^4} - \frac{4(u_{j,k+1}^{S})(\gamma v_{j,k+1}^{S} - 2\beta\sigma u_{j,k+1}^{S} w_{j,k+1}^{S})}{\alpha(1+v_{j,k+1}^{S})^2(\sigma+(u_{j,k+1}^{S})^2)^2}} , 0 \right),
$$

(3.14)

$$
b_{j,k+\frac{1}{2}}^{-} = \frac{\alpha}{2} \min \left(\frac{q_{j,k}^{N}}{(1+v_{j,k}^{N})^2} - \sqrt{\frac{(q_{j,k}^{N})^2}{(1+v_{j,k}^{N})^4} - \frac{4(u_{j,k}^{N})(\gamma v_{j,k}^{N} - 2\beta\sigma u_{j,k}^{N} w_{j,k}^{N})}{\alpha(1+v_{j,k}^{N})^2(\sigma+(u_{j,k}^{N})^2)^2}} \right. ,
$$
$$
\left. \frac{q_{j,k+1}^{S}}{(1+v_{j,k+1}^{S})^2} - \sqrt{\frac{(q_{j,k+1}^{S})^2}{(1+v_{j,k+1}^{S})^4} - \frac{4(u_{j,k+1}^{S})(\gamma v_{j,k+1}^{S} - 2\beta\sigma u_{j,k+1}^{S} w_{j,k+1}^{S})}{\alpha(1+v_{j,k+1}^{S})^2(\sigma+(u_{j,k+1}^{S})^2)^2}} , 0 \right),
$$

if all the expressions under the square roots in (3.14) are defined, and

$$b^+_{j,k+\frac{1}{2}} = \alpha \max\left(\frac{q^N_{j,k}}{(1 + v^N_{j,k})^2}, \frac{q^S_{j,k+1}}{(1 + v^S_{j,k+1})^2}, 0\right),$$

$$b^-_{j,k+\frac{1}{2}} = \alpha \min\left(\frac{q^N_{j,k}}{(1 + v^N_{j,k})^2}, \frac{q^S_{j,k+1}}{(1 + v^S_{j,k+1})^2}, 0\right),$$

otherwise. The cell averages of the reaction term are obtained using the midpoint rule and are given by:

$$\overline{R}^{(1)}_{j,k} = \rho \overline{u}_{j,k}\left(\frac{\delta(\overline{w}_{j,k})^2}{1 + (\overline{w}_{j,k})^2} - \overline{u}_{j,k}\right), \quad \overline{R}^{(2)}_{j,k} = \frac{\beta \overline{w}(\overline{u}_{j,k})^2}{\sigma + (\overline{u}_{j,k})^2} - \gamma \overline{u}_{j,k}\overline{v}_{j,k},$$

$$\overline{R}^{(3)}_{j,k} = \overline{R}^{(4)}_{j,k} = 0, \quad \overline{R}^{(5)}_{j,k} = -\frac{\kappa \overline{u}_{j,k}(\overline{w}_{j,k})^2}{1 + (\overline{w}_{j,k})^2}$$

where $\mathbf{R} = (R^{(1)}, R^{(2)}, R^{(3)}, R^{(4)}, R^{(5)})^T$.

Finally, as in Sect. 2, we take the numerical fluxes $(H^x)^{(2)}_{j+\frac{1}{2},k} \equiv (H^x)^{(4)}_{j+\frac{1}{2},k} \equiv (H^x)^{(5)}_{j+\frac{1}{2},k} \equiv 0$ and $(H^y)^{(2)}_{j,k+\frac{1}{2}} \equiv (H^y)^{(3)}_{j,k+\frac{1}{2}} \equiv (H^y)^{(5)}_{j,k+\frac{1}{2}} \equiv 0$ for all j, k, since the corresponding components of the $\mathbf{f}$ and $\mathbf{g}$ fluxes are zero. Here, $\mathbf{H} = (H^{(1)}, H^{(2)}, H^{(3)}, H^{(4)}, H^{(5)})^T$.

Example 4 (Cell density pattern formation in semi-solid medium.) We consider the following setup for the initial data:

$$u(x, y, 0) = \begin{cases} 5\cos^2\left(\frac{\pi\sqrt{x^2+y^2}}{4}\right), & \text{if } x^2 + y^2 \leq 4, \\ 0, & \text{otherwise,} \end{cases} \quad \begin{array}{l} v(x, y, 0) = 0, \\ w(x, y, 0) \equiv 1. \end{array} \quad (3.15)$$

The values of the parameters used are:

$$\begin{array}{llll} \alpha = 40, & d_u = 0.5, & \rho = 1.5, & \delta = 2, \quad d_v = 0.25, \\ \beta = 10, & \sigma = 100, & \gamma = 1, & d_w = 0.25, \quad \kappa = 0.005, \end{array} \quad (3.16)$$

and the IBVP (3.7)–(3.9), (3.15) and (3.16) is solved in the domain $[0, 30] \times [0, 30]$.

Unlike the Keller–Segel model, the chemotactic term in (3.7) contains a regularizing factor $1/(1 + v^2)$, which is expected to prevent a solution blowup. To the best of our knowledge, no analytic results on the global existence of the solution of (3.7)–(3.9) are available. However, the numerical results reported in [51,52] suggest that the solution of the IBVP (3.7)–(3.9), (3.15) and (3.16) may develop complicated spiky structures but would not blow up. Therefore, one may expect that designing a good numerical method for the considered IBVP would be easier than for the problems studied in the previous numerical examples. As in Sect. 3.1, we demonstrate here that a naïve

finite-difference approach may not work due to appearance of negative values of the computed cell density.

We begin with writing down a semi-discrete finite-difference scheme:

$$
\begin{cases}
\dfrac{du_{j,k}}{dt} = -\dfrac{H^x_{j+\frac{1}{2},k}(t) - H^x_{j-\frac{1}{2},k}(t)}{\Delta x} - \dfrac{H^y_{j,k+\frac{1}{2}}(t) - H^y_{j,k-\frac{1}{2}}(t)}{\Delta y} \\
\qquad + d_u \left[\dfrac{u_{j+1,k}(t) - 2u_{j,k}(t) + u_{j-1,k}(t)}{(\Delta x)^2} + \dfrac{u_{j,k+1}(t) - 2u_{j,k}(t) + u_{j,k-1}(t)}{(\Delta y)^2} \right], \\
\qquad + \rho u_{j,k}(t) \left(\delta \dfrac{w^2_{j,k}(t)}{1 + w^2_{j,k}(t)} - u_{j,k}(t) \right) \\
\dfrac{dv_{j,k}}{dt} = d_v \left[\dfrac{v_{j+1,k}(t) - 2v_{j,k}(t) + v_{j-1,k}(t)}{(\Delta x)^2} + \dfrac{v_{j,k+1}(t) - 2v_{j,k}(t) + v_{j,k-1}(t)}{(\Delta y)^2} \right] \\
\qquad + \beta \dfrac{w_{j,k}(t) u^2_{j,k}(t)}{\sigma + u^2_{j,k}(t)} - \gamma u_{j,k}(t) v_{j,k}(t) \\
\dfrac{dw_{j,k}}{dt} = d_w \left[\dfrac{w_{j+1,k}(t) - 2w_{j,k}(t) + w_{j-1,k}(t)}{(\Delta x)^2} + \dfrac{w_{j,k+1}(t) - 2w_{j,k}(t) + w_{j,k-1}(t)}{(\Delta y)^2} \right] \\
\qquad - \kappa u_{j,k}(t) \dfrac{w^2_{j,k}(t)}{1 + w^2_{j,k}(t)}.
\end{cases}
\tag{3.17}
$$

Here, $u_{j,k}(t)$, $v_{j,k}(t)$ and $w_{j,k}(t)$ denote the approximation of the point values $u(x_j, y_k, t)$, $v(x_j, y_k, t)$ and $w(x_j, y_k, t)$, respectively, and the centered fluxes are:

$$
\begin{aligned}
H^x_{j+\frac{1}{2},k}(t) &= \alpha \, \frac{u_{j+\frac{1}{2},k}(t)}{(1 + v_{j+\frac{1}{2},k}(t))^2} \cdot \frac{v_{j+1,k}(t) - v_{j,k}(t)}{\Delta x}, \\
H^y_{j,k+\frac{1}{2}}(t) &= \alpha \, \frac{u_{j,k+\frac{1}{2}}(t)}{(1 + v_{j+\frac{1}{2},k}(t))^2} \cdot \frac{v_{j,k+1}(t) - v_{j,k}(t)}{\Delta y},
\end{aligned}
\tag{3.18}
$$

where

$$
\begin{aligned}
u_{j+\frac{1}{2},k}(t) &= \frac{u_{j+1,k}(t) + u_{j,k}(t)}{2}, & v_{j+\frac{1}{2},k}(t) &= \frac{v_{j+1,k}(t) + v_{j,k}(t)}{2}, \\
u_{j,k+\frac{1}{2}}(t) &= \frac{u_{j,k+1}(t) + u_{j,k}(t)}{2}, & v_{j,k+\frac{1}{2}}(t) &= \frac{v_{j,k+1}(t) + v_{j,k}(t)}{2}.
\end{aligned}
\tag{3.19}
$$

The fully discrete finite-difference scheme is then obtained by applying an ODE solver to (3.17)–(3.19). In our numerical experiments, we have tested different ODE solvers and the obtained results did not depend on a particular choice of the time discretization.

We apply the above finite-difference scheme to the IBVP (3.7)–(3.9), (3.15) and (3.16). The cell densities at time $t = 6$ computed on a uniform grid $\Delta x = \Delta y = 1/5$ are plotted in Fig. 17. As one can see in the three-dimensional (3D) graph on the right, negative values already appear at this time even though the structure of the solution on the left looks reasonable (compare with the solution obtained by the proposed positivity preserving central-upwind scheme shown in Fig. 19). We then refine the grid to $\Delta x = \Delta y = 1/10$ and plot the computed cell densities in Fig. 18: the resolution increased but some of the density values are still negative. We expect that by further refining the mesh (while keeping the final time fixed) an accurate positive solution will
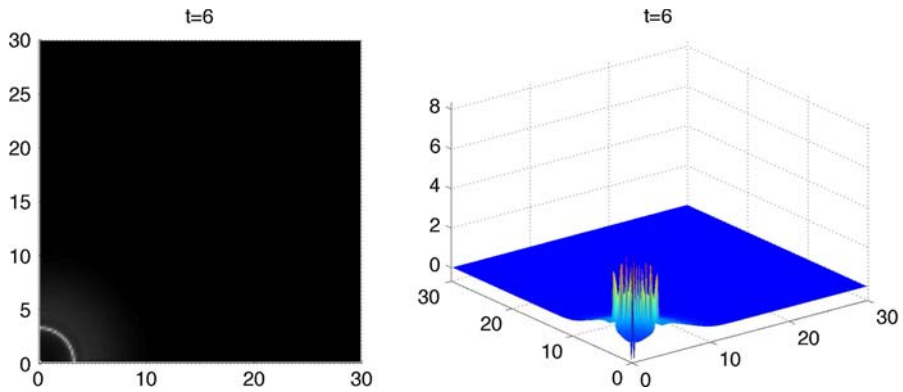
Fig. 17 Solution (u) of (3.7)–(3.9), (3.15) and (3.16) by the finite-difference scheme with $\Delta x = \Delta y = 1/5$
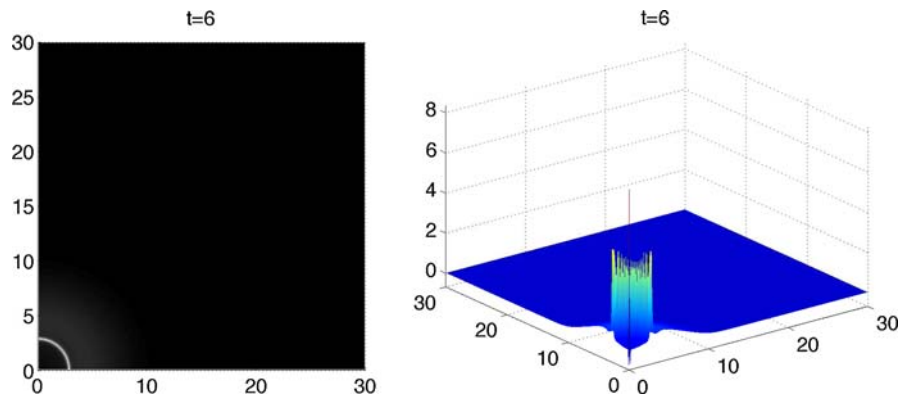
Fig. 18 Solution (u) of (3.7)–(3.9), (3.15) and (3.16) by the finite-difference scheme with $\Delta x = \Delta y = 1/10$
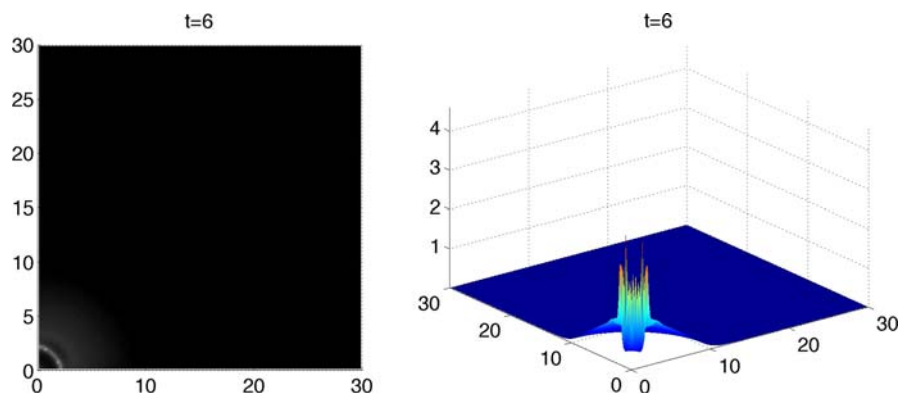
Fig. 19 Solution (u) of (3.10), (3.15) and (3.16) by the central-upwind scheme with $\Delta x = \Delta y = 1/5$

be captured by the described finite-difference scheme. However, the required mesh size may be impractical, especially for computing the solution at large times.

Next, we compute the solution of the same IBVP (3.7)–(3.9), (3.15) and (3.16) at time $t = 6$ using the positivity preserving central-upwind scheme, applied to the system (3.10). For comparison, we perform computations on the same set of uniform grids and present the results in Figs. 19 and 20. As anticipated, no negative numerical values have been developed.

We then continue both the finite-difference and central-upwind computations to times $t = 12, 24, 18$ and 30. The finite-difference scheme keeps producing negative values of cell densities. Unlike the Keller-Segel case, the magnitude of these negative values does not increase in time, but they propagate and slowly destroy the spiky pattern in the computed solution—see Figs. 21 and 22 and compare with the results obtained by the central-upwind scheme shown in Figs. 23 and 24. We would also like to point out that the considered model is very sensitive to the choice of the parameters in (3.16), but the qualitative behavior of the central-upwind results is in the spirit of the experimental data from [7,8] and the numerical results reported in [51,52].

3.3 Model of chemotactic bacteria patterns in liquid medium

In this section, we consider a special case of the system studied in Sect. 3.2, which describes bacteria patterns in the liquid medium that contains sufficient nutrients for the bacteria. According to [50] (see also [51]), in this case, the coefficients ρ and γ are equal to zero and the nutrient concentration w is assumed to be constant so that the system (3.7)–(3.9) reduces to:

$$u_t + \alpha \nabla \cdot \left[\frac{u}{(1+v)^2} \nabla v \right] = d_u \Delta u, \tag{3.20}$$

$$v_t = d_v \Delta v + \beta \frac{wu^2}{\sigma + u^2}. \tag{3.21}$$
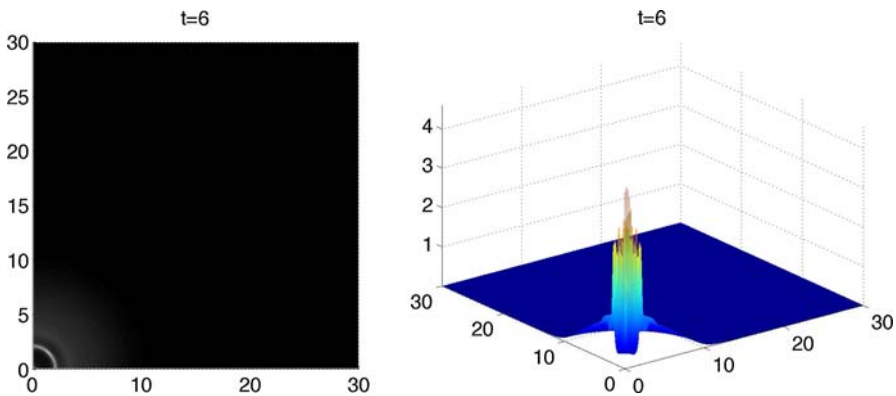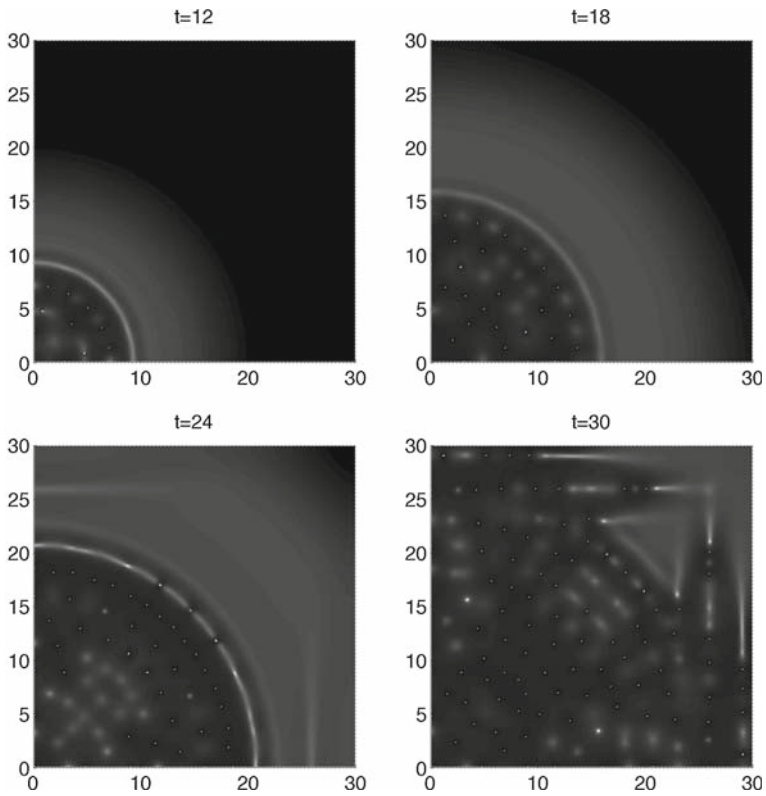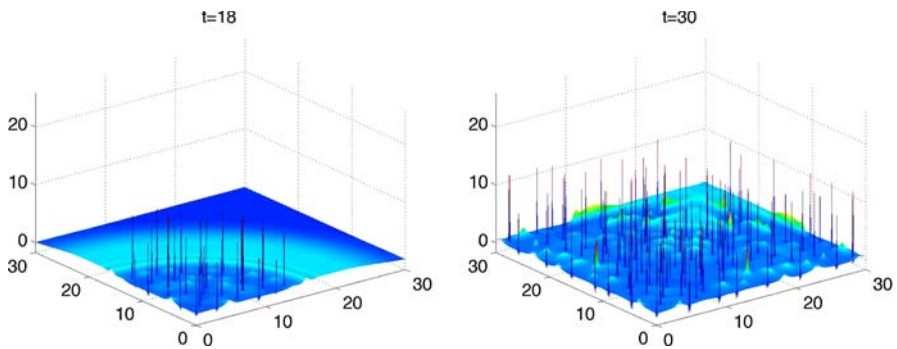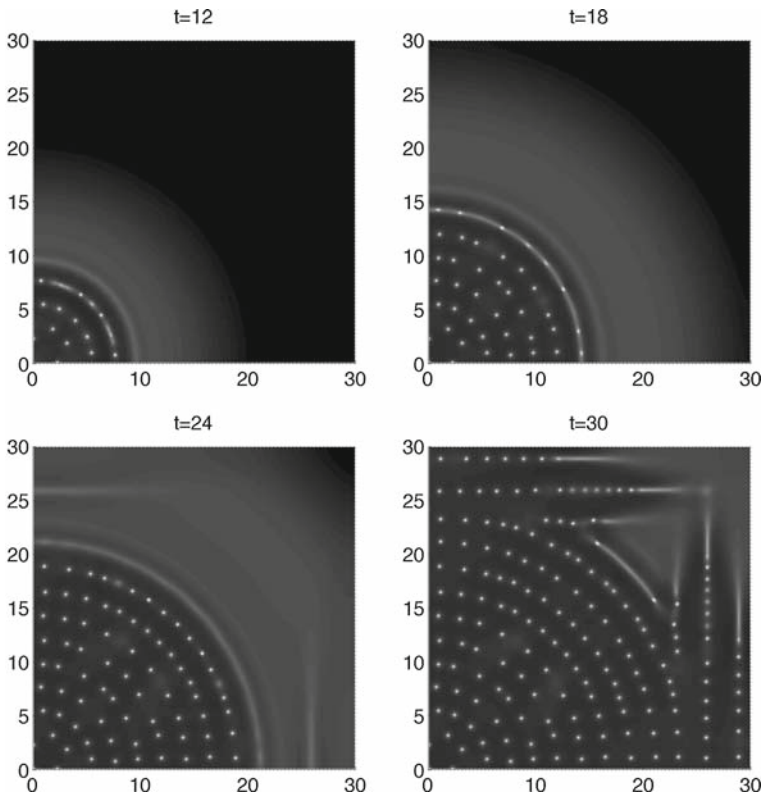

Fig. 20 Solution (u) of (3.10), (3.15) and (3.16) by the central-upwind scheme with $\Delta x = \Delta y = 1/10$
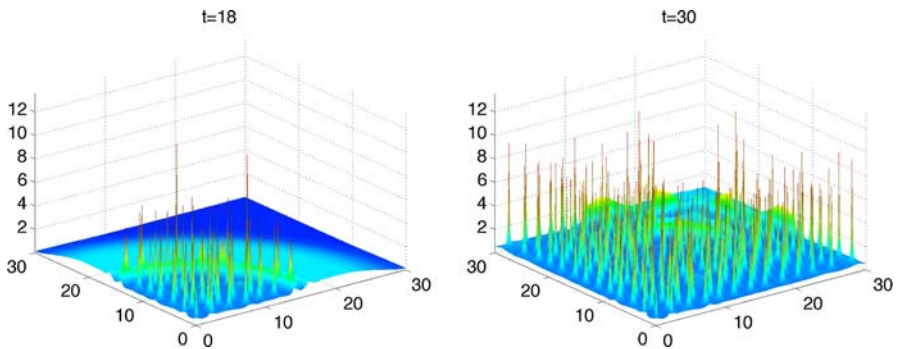
Fig. 21 Solution (u) of (19) and (20), (3.15) and (3.16) by the finite-difference scheme with $\Delta x = \Delta y = 1/10$

Fig. 22 Three-dimensional plot of the solution from Fig. 21 at times $t = 18$ and $t = 30$

Fig. 23 Solution (u) of (3.10), (3.15) and (3.16) by the central-upwind scheme with $\Delta x = \Delta y = 1/10$

Fig. 24 Three-dimensional plot of the solution from Fig. 23 at times $t = 18$ and $t = 30$

As before, α, d_u, d_v, β, and σ are positive constants.

As in the previous sections, we first differentiate equation (3.21) with respect to x and y, introduce the notation $p := v_x$, $q := v_y$, and rewrite the system (3.20) and (3.21) as follows:

$$\begin{cases} u_t + \left(\dfrac{\alpha up}{(1+v)^2}\right)_x + \left(\dfrac{\alpha uq}{(1+v)^2}\right)_y = d_u(u_{xx} + u_{yy}), \\[2mm] v_t = d_v(v_{xx} + v_{yy}) + \dfrac{\beta wu^2}{\sigma + u^2}, \\[2mm] p_t + \left(\dfrac{\beta w\sigma}{\sigma + u^2}\right)_x = d_v(p_{xx} + p_{yy}), \\[2mm] q_t + \left(\dfrac{\beta w\sigma}{\sigma+u^2}\right)_y = d_v(q_{xx} + q_{yy}), \end{cases}$$

or in the flux form as:

$$\mathbf{U}_t + \mathbf{f}(\mathbf{U})_x + \mathbf{g}(\mathbf{U})_y = \Lambda(\mathbf{U}_{xx} + \mathbf{U}_{yy}) + \mathbf{R}(\mathbf{U}). \tag{3.22}$$

Here, $\mathbf{U} := (u, v, p, q)^T$, $\mathbf{f}(\mathbf{U}) := \left(\frac{\alpha up}{(1+v)^2}, 0, \frac{\beta w\sigma}{\sigma+u^2}, 0\right)^T$, $\mathbf{g}(\mathbf{U}) := \left(\frac{\alpha uq}{(1+v)^2}, 0, 0, \frac{\beta w\sigma}{\sigma+u^2}\right)^T$, $\Lambda := \mathrm{diag}(d_u, d_v, d_v, d_v)$, and $\mathbf{R}(\mathbf{U}) := (0, \frac{\beta wu^2}{\sigma+u^2}, 0, 0)^T$. The eigenvalues of the Jacobians $\frac{\partial \mathbf{f}}{\partial \mathbf{U}}$ and $\frac{\partial \mathbf{g}}{\partial \mathbf{U}}$ are:

$$\lambda_{1,2}^{\mathbf{f}} = \frac{\alpha}{2(1+v)^2}\left(p \pm \sqrt{p^2 - \frac{8\beta w\sigma u^2(1+v)^2}{\alpha(\sigma+u^2)^2}}\right), \quad \lambda_3^{\mathbf{f}} = \lambda_4^{\mathbf{f}} = 0 \tag{3.23}$$

and

$$\lambda_{1,2}^{\mathbf{g}} = \frac{\alpha}{2(1+v)^2}\left(q \pm \sqrt{q^2 - \frac{8\beta w\sigma u^2(1+v)^2}{\alpha(\sigma+u^2)^2}}\right), \quad \lambda_3^{\mathbf{g}} = \lambda_4^{\mathbf{g}} = 0, \tag{3.24}$$

respectively.

As in the previously considered systems, the eigenvalues may be complex so that the convective part of the system (3.22) is conditionally hyperbolic. Therefore, the one-sided local speeds are computed depending on the sign of the expressions under the square roots in (3.23) and (3.24). Namely, the x-speeds are:

$$a_{j+\frac{1}{2},k}^+ = \frac{\alpha}{2}\max\left(\frac{p_{j,k}^{\mathrm{E}}}{(1+v_{j,k}^{\mathrm{E}})^2} + \sqrt{\frac{(p_{j,k}^{\mathrm{E}})^2}{(1+v_{j,k}^{\mathrm{E}})^4} - \frac{8\beta w\sigma(u_{j,k}^{\mathrm{E}})^2}{\alpha(1+v_{j,k}^{\mathrm{E}})^2(\sigma+(u_{j,k}^{\mathrm{E}})^2)^2}},\right.$$
$$\left.\frac{p_{j+1,k}^{\mathrm{W}}}{(1+v_{j+1,k}^{\mathrm{W}})^2} + \sqrt{\frac{(p_{j+1,k}^{\mathrm{W}})^2}{(1+v_{j+1,k}^{\mathrm{W}})^4} - \frac{8\beta w\sigma(u_{j+1,k}^{\mathrm{W}})^2}{\alpha(1+v_{j+1,k}^{\mathrm{W}})^2(\sigma+(u_{j+1,k}^{\mathrm{W}})^2)^2}},\, 0\right),$$

$$\tag{3.25}$$

$$a_{j+\frac{1}{2},k}^- = \frac{\alpha}{2}\min\left(\frac{p_{j,k}^{\mathrm{E}}}{(1+v_{j,k}^{\mathrm{E}})^2} - \sqrt{\frac{(p_{j,k}^{\mathrm{E}})^2}{(1+v_{j,k}^{\mathrm{E}})^4} - \frac{8\beta w\sigma(u_{j,k}^{\mathrm{E}})^2}{\alpha(1+v_{j,k}^{\mathrm{E}})^2(\sigma+(u_{j,k}^{\mathrm{E}})^2)^2}},\right.$$

$$\frac{p^{\mathrm{W}}_{j+1,k}}{(1+v^{\mathrm{W}}_{j+1,k})^2} - \sqrt{\frac{(p^{\mathrm{W}}_{j+1,k})^2}{(1+v^{\mathrm{W}}_{j+1,k})^4} - \frac{8\beta w\sigma(u^{\mathrm{W}}_{j+1,k})^2}{\alpha(1+v^{\mathrm{W}}_{j+1,k})^2(\sigma+(u^{\mathrm{W}}_{j+1,k})^2)^2}}, \; 0 \Bigg),$$

if all the expressions under the square roots in (3.25) are defined, and

$$a^{+}_{j+\frac{1}{2},k} = \alpha \max\left(\frac{p^{\mathrm{E}}_{j,k}}{(1+v^{\mathrm{E}}_{j,k})^2}, \frac{p^{\mathrm{W}}_{j+1,k}}{(1+v^{\mathrm{W}}_{j+1,k})^2}, \; 0\right),$$

$$a^{-}_{j+\frac{1}{2},k} = \alpha \min\left(\frac{p^{\mathrm{E}}_{j,k}}{(1+v^{\mathrm{E}}_{j,k})^2}, \frac{p^{\mathrm{W}}_{j+1,k}}{(1+v^{\mathrm{W}}_{j+1,k})^2}, \; 0\right),$$

otherwise; and the y-speeds are:

$$b^{+}_{j,k+\frac{1}{2}} = \frac{\alpha}{2} \max\left(\frac{q^{\mathrm{N}}_{j,k}}{(1+v^{\mathrm{N}}_{j,k})^2} + \sqrt{\frac{(q^{\mathrm{N}}_{j,k})^2}{(1+v^{\mathrm{N}}_{j,k})^4} - \frac{8\beta w\sigma(u^{\mathrm{N}}_{j,k})^2}{\alpha(1+v^{\mathrm{N}}_{j,k})^2(\sigma+(u^{\mathrm{N}}_{j,k})^2)^2}}\, ,\right.$$

$$\left. \frac{q^{\mathrm{S}}_{j,k+1}}{(1+v^{\mathrm{S}}_{j,k+1})^2} + \sqrt{\frac{(q^{\mathrm{S}}_{j,k+1})^2}{(1+v^{\mathrm{S}}_{j,k+1})^4} - \frac{8\beta w\sigma(u^{\mathrm{S}}_{j,k+1})^2}{\alpha(1+v^{\mathrm{S}}_{j,k+1})^2(\sigma+(u^{\mathrm{S}}_{j,k+1})^2)^2}}, \; 0\right),$$

$$\text{(3.26)}$$

$$b^{-}_{j,k+\frac{1}{2}} = \frac{\alpha}{2} \min\left(\frac{q^{\mathrm{N}}_{j,k}}{(1+v^{\mathrm{N}}_{j,k})^2} - \sqrt{\frac{(q^{\mathrm{N}}_{j,k})^2}{(1+v^{\mathrm{N}}_{j,k})^4} - \frac{8\beta w\sigma(u^{\mathrm{N}}_{j,k})^2}{\alpha(1+v^{\mathrm{N}}_{j,k})^2(\sigma+(u^{\mathrm{N}}_{j,k})^2)^2}}\, ,\right.$$

$$\left. \frac{q^{\mathrm{S}}_{j,k+1}}{(1+v^{\mathrm{S}}_{j,k+1})^2} - \sqrt{\frac{(q^{\mathrm{S}}_{j,k+1})^2}{(1+v^{\mathrm{S}}_{j,k+1})^4} - \frac{8\beta w\sigma(u^{\mathrm{S}}_{j,k+1})^2}{\alpha(1+v^{\mathrm{S}}_{j,k+1})^2(\sigma+(u^{\mathrm{S}}_{j,k+1})^2)^2}}, \; 0\right),$$

if all the expressions under the square roots in (3.26) are defined, and

$$b^{+}_{j,k+\frac{1}{2}} = \alpha \max\left(\frac{q^{\mathrm{N}}_{j,k}}{(1+v^{\mathrm{N}}_{j,k})^2}, \frac{q^{\mathrm{S}}_{j,k+1}}{(1+v^{\mathrm{S}}_{j,k+1})^2}, \; 0\right),$$

$$b^{-}_{j,k+\frac{1}{2}} = \alpha \min\left(\frac{q^{\mathrm{N}}_{j,k}}{(1+v^{\mathrm{N}}_{j,k})^2}, \frac{q^{\mathrm{S}}_{j,k+1}}{(1+v^{\mathrm{S}}_{j,k+1})^2}, \; 0\right),$$

otherwise. The cell averages of the reaction term are:

$$\overline{R}^{(1)}_{j,k} = 0, \quad \overline{R}^{(2)}_{j,k} = \frac{\beta w(\overline{u}_{j,k})^2}{\sigma+(\overline{u}_{j,k})^2}, \quad \overline{R}^{(3)}_{j,k} = \overline{R}^{(4)}_{j,k} = 0.$$

Finally, as in Sects. 2 and 3.2, we take $(H^x)^{(2)}_{j+\frac{1}{2},k} \equiv (H^x)^{(4)}_{j+\frac{1}{2},k} \equiv 0$ and $(H^y)^{(2)}_{j,k+\frac{1}{2}}$
$\equiv (H^y)^{(3)}_{j,k+\frac{1}{2}} \equiv 0$ for all j, k, since the corresponding components of the **f** and **g** fluxes are zero.

Example 5 (Cell density pattern formation in liquid medium.) In this example, we apply the derived scheme to the system (3.22) subject to the following initial data:

$$u(x, y, 0) = 0.9 + 0.2\sigma(x, y), \quad v(x, y, 0) = 0, \tag{3.27}$$

where σ is a random variable uniformly distributed on [0, 1]. The IBVP is solved in the domain $[0, 10] \times [0, 10]$ and the parameters are chosen as:

$$\alpha = 80, \quad d_v = 0.33, \quad d_u = \beta = \sigma = w = 1.$$

In Figs. 25 and 26, we plot the computed solution (cell densities) at various times. We would like to notice that the obtained results match well with both experimental data from [7,8] and the numerical results reported in [50]. This confirms the robustness of the proposed central-upwind scheme.
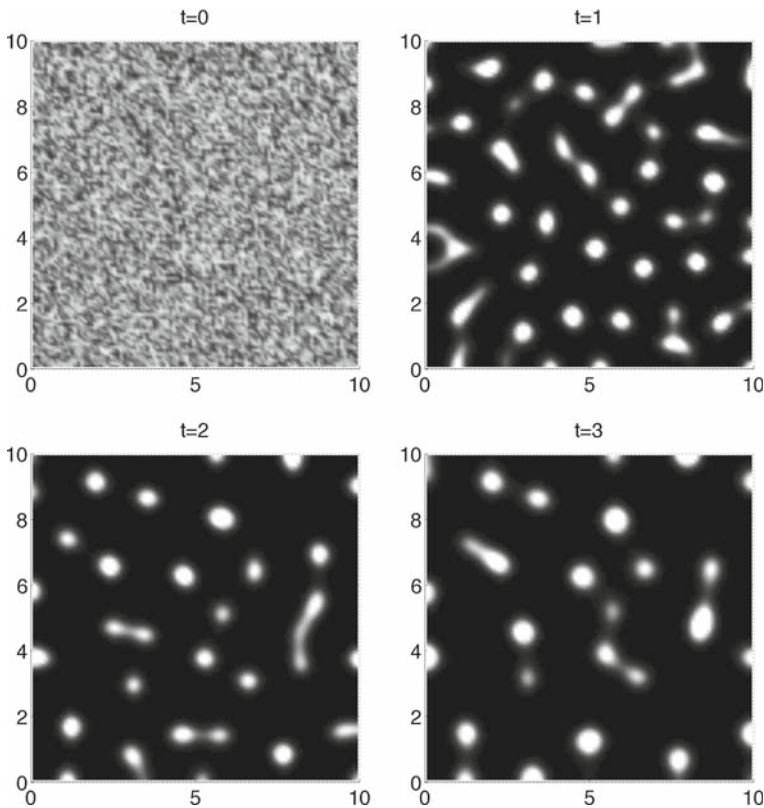
Fig. 25 Solution (u) of (3.22), (3.27) by the central-upwind scheme with $\Delta x = \Delta y = 1/10$
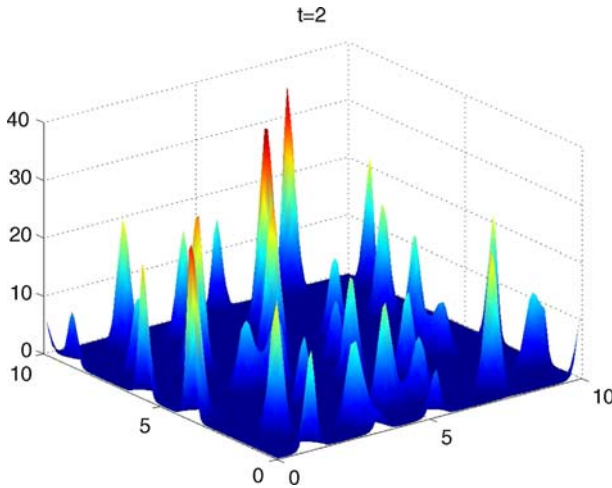
Fig. 26 Three-dimensional plot of the solution from Fig. 25 at time $t = 2$

3.4 A haptotaxis model

In the final section, we apply the designed central-upwind scheme to a haptotaxis model proposed in [2,10,11], see also [5,53]. The model can be described by the 2D system of advection-reaction-diffusion equations:

$$u_t + \nabla \cdot (\chi(v)u\nabla v) = d_u \Delta u - \psi(x, y, w)u + \rho(x, y, w)u, \qquad (3.28)$$

$$v_t = -\alpha(x, y)mv, \qquad (3.29)$$

$$m_t = d_m \Delta m + \delta(x, y)u - \beta(x, y)m, \qquad (3.30)$$

$$w_t = d_w \Delta w + \gamma(x, y)v - e(x, y)w - \eta(x, y, u)w. \qquad (3.31)$$

This system models a process of tumor invasion into surrounding healthy tissue. The dependent variables in (3.28)–(3.31) are: the density of tumor cells, $u(x, y, t)$, the density of extracellular matrix macromolecules, $v(x, y, t)$, the concentration of matrix degradative enzyme, $m(x, y, t)$, and the concentration of oxygen ($w(x, y, t)$). The parameters $\chi(v), d_u, \psi(x, y, w), \rho(x, y, w), \alpha(x, y), d_m, \delta(x, y), \beta(x, y), d_w, \gamma(x, y), \eta(x, y, u)$, and $e(x, y)$ are specified in the numerical example below.
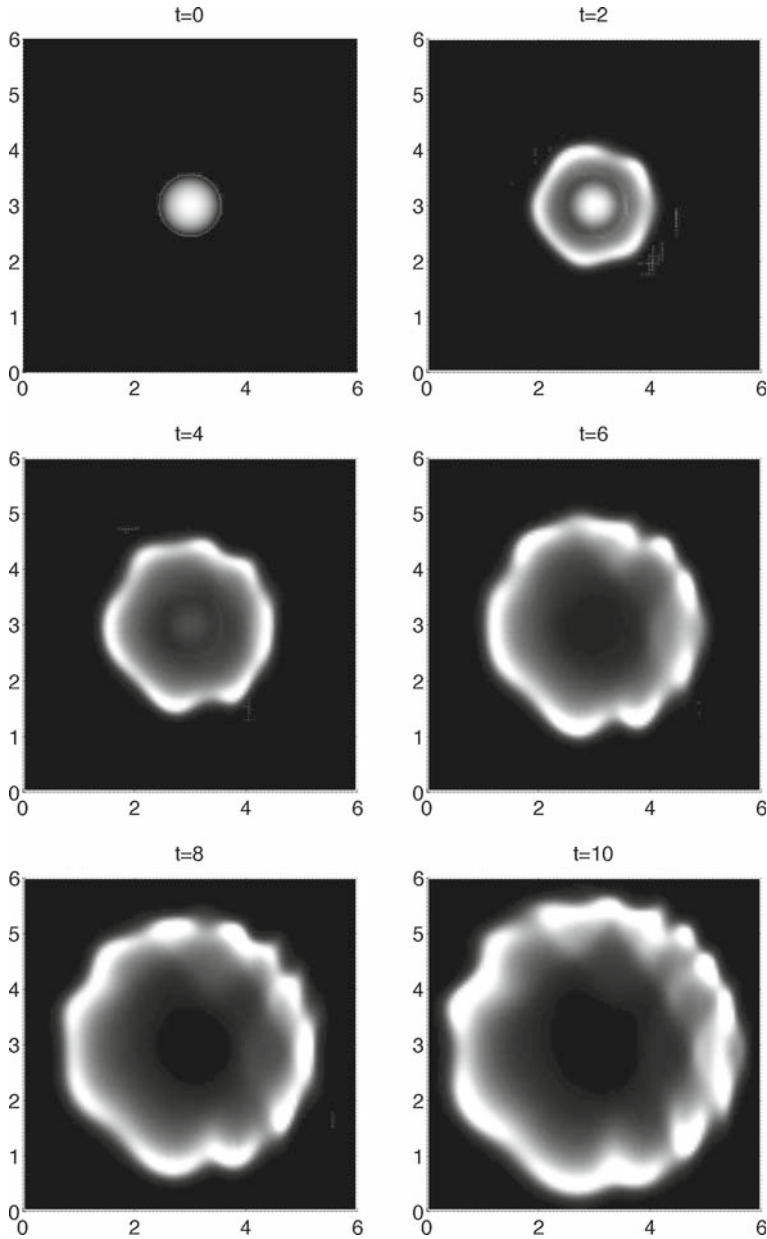
As before, we begin with differentiating (3.29) with respect to x and y and denote $p := v_x$ and $q := v_y$. Then the modified system reads:

$$\mathbf{U}_t + \mathbf{f}(\mathbf{U})_x + \mathbf{g}(\mathbf{U})_y = \Lambda(\mathbf{U}_{xx} + \mathbf{U}_{yy}) + \mathbf{R}(\mathbf{U}), \qquad (3.32)$$

where

$\mathbf{U} := (u, v, p, q, m, w)^T, \ \Lambda := \mathrm{diag}(d_u, 0, 0, 0, d_m, d_w),$
$\mathbf{f}(\mathbf{U}) := (\chi(v)up, 0, \alpha(x, y)mv, 0, 0, 0)^T, \mathbf{g}(\mathbf{U}) := (\chi(v)uq, 0, 0, \alpha(x, y)mv, 0, 0)^T,$

Fig. 27 Solution (u) of (3.32) and (3.34) by the central-upwind scheme with $\Delta x = \Delta y = 1/100$

$$\mathbf{R(U)} := (-\psi(x, y, w)u + \rho(x, y, w)u, -\alpha(x, y)mv, 0, 0, \delta(x, y)u - \beta(x, y)m,$$

$$\gamma(x, y)v - \eta(x, y, u)w - e(x, y)w)^T.$$

The eigenvalues of the Jacobians of $\frac{\partial \mathbf{f}}{\partial \mathbf{U}}$ and $\frac{\partial \mathbf{g}}{\partial \mathbf{U}}$ are:

$$\lambda_1^{\mathbf{f}} = \chi(v)p, \quad \lambda_2^{\mathbf{f}} = \cdots = \lambda_6^{\mathbf{f}} = 0, \quad \text{and} \quad \lambda_1^{\mathbf{g}} = \chi(v)q, \quad \lambda_2^{\mathbf{g}} = \cdots = \lambda_6^{\mathbf{g}} = 0, \quad (3.33)$$

respectively. Unlike the previously considered chemotaxis models, all the eigenvalues are real now, and thus the convective part of the haptotaxis system (3.32) is hyperbolic. Therefore, the one-sided local speeds can be taken as the largest/smallest eigenvalues of the corresponding Jacobians.

The semi-discrete central-upwind scheme can be then applied to the system (3.32) in a straightforward manner, and we leave it to the reader to fill in the remaining details in the scheme construction. We would only like to mention that in (3.32), as in the previously considered systems, there are several zero flux components. Therefore, we take the corresponding numerical fluxes to be $(H^x)^{(2)} \equiv (H^x)^{(4)} \equiv (H^x)^{(5)} \equiv (H^x)^{(6)} \equiv 0$ and $(H^y)^{(2)} \equiv (H^y)^{(3)} \equiv (H^y)^{(5)} \equiv (H^y)^{(6)} \equiv 0$.
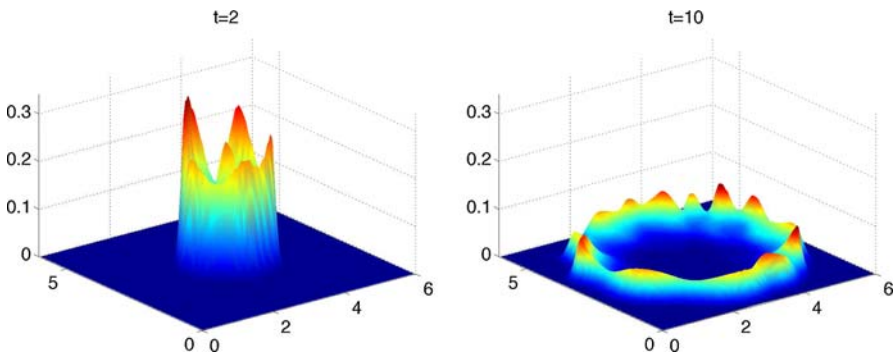
Example 6 (Constant haptotaxis sensitivity.) We apply the central-upwind scheme to the system (3.32) with the following choice of parameters:

$$\chi(v) \equiv 0.4, \; d_u = 0.01, \; \psi(x, y, w) \equiv 1, \; \rho(x, y, w) = \frac{2w}{1 + w},$$
$$\alpha(x, y) \equiv 5, \; d_m = 0.01,$$
$$\delta(x, y) \equiv 1, \; \beta(x, y) \equiv 0.01, \; d_w = 0.01, \; \gamma(x, y) \equiv 5,$$
$$\eta(x, y, u) = \frac{2u}{1 + u}, \; e(x, y) \equiv 1.$$

The initial data are given by:

$$u(x, y, 0) = 5 \max\{0.3 - (x - 3)^2 - (y - 3)^2, 0\},$$
$$v(x, y, 0) = 0.05 \cos\left(\frac{5\pi x^2}{18}\right) \sin\left(\frac{13\pi y^2}{72}\right) + 0.3, \quad (3.34)$$
$$m(x, y, 0) = u(x, y, 0), \; w(x, y, 0) = 4 v(x, y, 0),$$

and the IBVP is solved in the domain $[0, 6] \times [0, 6]$.

Fig. 28 Three-dimensional plot of the solutions from Fig. 27 at times $t = 2$ and $t = 10$

Tumor cell densities computed at different times are shown in Figs. 27 and 28. The results seem to be in a very good agreement with the results reported in [53], which confirms the robustness of the proposed central-upwind scheme.

References

1. Adler, J.: Chemotaxis in bacteria. Ann. Rev. Biochem. **44**, 341–356 (1975)
2. Anderson, A.R.A.: A hybrid mathematical model of solid tumor invasion: the importance of cell adhesion. Math. Med. Biol. IMA J. **22**, 163–186 (2005)
3. Ascher, U.M., Ruuth, S.J., Spiteri, R.J.: Implicit-explicit Runge–Kutta methods for time-dependent partial differential equations. Special issue on time integration (Amsterdam, 1996). Appl. Numer. Math. **25**, 151–167 (1997)
4. Ascher, U.M., Ruuth, S.J., Wetton, B.T.R.: Implicit-explicit methods for time-dependent partial differential equations. SIAM J. Numer. Anal. **32**, 797–823 (1995)
5. Ayati, B.P., Webb, G.F., Anderson, A.R.A.: Computational methods and results for structured multiscale models of tumor invasion. Multiscale Model. Simul. **5**, 1–20 (2006)
6. Bonner, J.T.: The Cellular Slime Molds, 2nd edn. Princeton University Press, Princeton (1967)
7. Budrene, E.O., Berg, H.C.: Complex patterns formed by motile cells of escherichia coli. Nature **349**, 630–633 (1991)
8. Budrene, E.O., Berg, H.C.: Dynamics of formation of symmetrical patterns by chemotactic bacteria. Nature **376**, 49–53 (1995)
9. Calvez, V., Carrillo, J.A.: Volume effects in the Keller–Segel model: energy estimates preventing blow-up. J. Math. Pures Appl. **86**, 155–175 (2006)
10. Carter, S.B.: Principles of cell motility: the direction of cell movement and cancer invasion. Nature **208**, 1183–1187 (1965)
11. Carter, S.B.: Haptotaxis and the mechanism of cell motility. Nature **213**, 256–260 (1967)
12. Chertock, A., Kurganov, A., Petrova, G.: Fast explicit operator splitting method for convection-diffusion equations. Int. J. Numer. Methods Fluids (2008, in press)
13. Childress, S., Percus, J.K.: Nonlinear aspects of chemotaxis. Math. Biosci. **56**, 217–237 (1981)
14. Cohen, M.H., Robertson, A.: Wave propagation in the early stages of aggregation of cellular slime molds. J. Theor. Biol. **31**, 101–118 (1971)
15. Filbet, F.: A finite volume scheme for the Patlak-Keller-Segel chemotaxis model. Numer. Math. **104**, 457–488 (2006)
16. Godlewski, E., Raviart, P.-A.: Numerical Approximation of Hyperbolic Systems of Conservation Laws. Springer, New York (1996)
17. Godunov, S.K.: A difference method for numerical calculation of discontinuous solutions of the equations of hydrodynamics. Mat. Sb. **47**, 271–306 (1959)
18. Gottlieb, S., Shu, C.-W., Tadmor, E.: High order time discretization methods with the strong stability property. SIAM Rev. **43**, 89–112 (2001)
19. Herrero, M.A., Velázquez, J.J.L.: A blow-up mechanism for a chemotaxis model. Ann. Sc. Norm. Super. **24**, 633–683 (1997)
20. Higueras, I., Roldán, T.: Positivity-preserving and entropy-decaying IMEX methods. In: Ninth International Conference Zaragoza-Pau on Applied Mathematics and Statistics. Monogr. Semin. Mat. Garcia Galdeano, vol. 33, pp. 129–136. Prensas University Zaragoza, Zaragoza (2006)
21. Hillen, T., Painter, K.J.: Global existence for a parabolic chemotaxis model with prevention of overcrowding. Adv. Appl. Math. **26**, 280–301 (2001)
22. Horstmann, D.: From 1970 until now: the Keller–Segel model in chemotaxis and its consequences I. Jahresber. DMV **105**, 103–165 (2003)
23. Horstmann, D.: From 1970 until now: the Keller–Segel model in chemotaxis and its consequences II. Jahresber. DMV **106**, 51–69 (2004)

24. Hundsdorfer, W., Verwer, J.: Numerical solution of time-dependent advection-diffusion-reaction equations. Springer Series in Computational Mathematics, vol. 33. Springer, Berlin (2003)
25. Keller, E.F., Segel, L.A.: Initiation of slime mold aggregation viewed as an instability. J. Theor. Biol. **26**, 399–415 (1970)
26. Keller, E.F., Segel, L.A.: Model for chemotaxis. J. Theor. Biol. **30**, 225–234 (1971)
27. Keller, E.F., Segel, L.A.: Treveling bands of chemotactic bacteria: a theoretical analysis. J. Theor. Biol. **30**, 235–248 (1971)
28. Kröner, D.: Numerical Schemes for Conservation Laws. Wiley, Chichester (1997)
29. Kurganov, A.: Central-upwind schemes for balance laws. Application to the Broadwell model. In: Finite Volumes for Complex Applications, III (Porquerolles, 2002), pp. 351–358. Hermes Sci. Publ., Paris (2002)
30. Kurganov, A., Levy, D.: Central-upwind schemes for the Saint–Venant system. M2AN Math. Model. Numer. Anal. **36**, 397–425 (2002)
31. Kurganov, A., Lin, C.-T.: On the reduction of numerical dissipation in central-upwind schemes. Commun. Comput. Phys. **2**, 141–163 (2007)
32. Kurganov, A., Noelle, S., Petrova, G.: Semi-discrete central-upwind schemes for hyperbolic conservation laws and Hamilton–Jacobi equations. SIAM J. Sci. Comput. **21**, 707–740 (2001)
33. Kurganov, A., Petrova, G.: A second-order well-balanced positivity preserving central-upwind scheme for the Saint-Venant system. Commun. Math. Sci. **5**, 133–160 (2007)
34. Kurganov, A., Tadmor, E.: New high-resolution central schemes for nonlinear conservation laws and convection-diffusion equations. J. Comput. Phys. **160**, 241–282 (2000)
35. van Leer, B.: Towards the ultimate conservative difference scheme, V. a second order sequel to Godunov's method. J. Comput. Phys. **32**, 101–136 (1979)
36. LeVeque, R.: Finite volume methods for hyperbolic problems. Cambridge Texts in Applied Mathematics. Cambridge University Press, London (2002)
37. Lie, K.-A., Noelle, S.: On the artificial compression method for second-order nonoscillatory central difference schemes for systems of conservation laws. SIAM J. Sci. Comput. **24**, 1157–1174 (2003)
38. Lin, C.-S., Ni, W.-M., Takagi, I.: Large amplitude stationary solutions to a chemotaxis system. J. Differ. Equ. **72**, 1–27 (1988)
39. Manoussaki, D.: A mechanochemical model of angiogenesis and vasculogenesis. M2AN Math. Model. Numer. Anal. **37**, 581–599 (2003)
40. Marrocco, A.: 2D simulation of chemotaxis bacteria aggregation. M2AN Math. Model. Numer. Anal. **37**, 617–630 (2003)
41. Nanjundiah, V.: Chemotaxis, signal relaying and aggregation morphology. J. Theor. Biol. **42**, 63–105 (1973)
42. Nessyahu, H., Tadmor, E.: Non-oscillatory central differencing for hyperbolic conservation laws. J. Comput. Phys. **87**, 408–463 (1990)
43. Pareschi, L., Russo, G.: Implicit-Explicit Runge–Kutta schemes and applications to hyperbolic systems with relaxation. J. Sci. Comput. **25**, 129–155 (2005)
44. Patlak, C.S.: Random walk with persistence and external bias. Bull. Math: Biophys. **15**, 311–338 (1953)
45. Perthame, B.: Transport equations in biology. Frontiers in Mathematics. Birkhäuser, Basel (2007)
46. Prescott, L.M., Harley, J.P., Klein, D.A.: Microbiology, 3rd edn. Wm. C. Brown Publishers, Chicago (1996)
47. Samarskii, A.A., Gulin, A.V.: Ustoichivost raznostnykh skhem (Russian) [Stability of difference schemes], 2nd edn. Editorial URSS, Moscow (2004)
48. Saito, N.: Conservative upwind finite-element method for a simplified Keller-Segel system modelling chemotaxis. IMA J. Numer. Anal. **27**, 332–365 (2007)
49. Sweby, P.K.: High resolution schemes using flux limiters for hyperbolic conservation laws. SIAM J. Numer. Anal. **21**, 995–1011 (1984)
50. Tyson, R., Lubkin, S.R., Murray, J.D.: Model and analysis of chemotactic bacterial patterns in a liquid medium. J. Math. Biol. **38**, 359–375 (1999)
51. Tyson, R., Lubkin, S.R., Murray, J.D.: A minimal mechanism for bacterial pattern formation. Proc. Roy. Soc. Lond. B **266**, 299–304 (1999)
52. Tyson, R., Stern, L.G., LeVeque, R.J.: Fractional step methods applied to a chemotaxis model. J. Math. Biol. **41**, 455–475 (2000)
53. Walker, C., Webb, G.F.: Global Existence of classical solutions for a haptotaxis model (preprint)
54. Woodward, D., Tyson, R., Myerscough, M., Murray, J., Budrene, E., Berg, H.: Spatio-temporal patterns generated by S. typhimurium. Biophys. J. **68**, 2181–2189 (1995)